Chapter 3.
FLUID FLOW.
September_11_2016.

3.1. Introduction. Fluid flow in hydrothermal systems.

Fluids in the form of aqueous solutions, solutions rich in CO_2, NaCl or hydrocarbons play an important role in hydrothermal systems (Fyfe et al., 1978). They influence the strength of deforming materials both through reactions with chemical bonds and through the *effective stress principle*; they facilitate deformation through dissolution and deposition of minerals. Fluids directly contribute to mineralisation through the supply of H^+ and $(OH)^-$ for mineral reactions (Austrheim, 1987; John and Schenk, 2003) and carry the essential ingredients that ultimately make an ore deposit. They have a profound effect on the rates of mineral reactions and coupled deformation rates (Rubie, 1998; Wintsch and Yi, 2002). Although fluids are important in retrograde metamorphism and in devolatilisation reactions the extreme behaviour is in metasomatic and mineralising systems where the fluids not only carry reactive ions that generate alteration assemblages and the mineral deposits themselves but *advect* the heat necessary to initiate and drive the reacting system. In this chapter we outline the mechanics of fluid generation and transport through the crust, discuss the factors that drive fluid flow and consider the coupling of fluid flow with heat transport. We discuss the thermodynamics of fluid advection in deforming rocks, the relevance of mean stress in driving fluid flow, critical behaviour of crustal flow systems and complete the chapter with an overview of crustal plumbing systems.

The important questions are: *What role does fluid flow play in the evolution of hydrothermal systems? What is the time integrated volume of fluid that passes through a rock during metasomatism (Yardley, 2009)? Are there parts of the system that remain dry (Thompson, 1983; Yardley and Valley, 1997)? What are the processes that drive fluid flow during metasomatism? In particular, how are meteoric waters driven into the deep crust (Fricke et al., 1992; Yardley et al., 1993; Cartwright et al., 1994; Munz et al., 1995)? What is the role of mean stress in driving fluid flow? Is convection an important process in the deep crust (Etheridge et al., 1983)? Can convection operate in a system with upward flow-through (Wood and Walther, 1986; Oliver, 1996)? How important are relatively impermeable "caps" and "seals" in hydrothermal systems (Etheridge et al., 1983; Sibson, 1994)? Is flow up, down or sideways? Is flow up or down temperature gradients? How important is fluid focussing (Ague, 2011)? What are the critical aspects of crustal plumbing systems that control where a mineralising system will form?* The aim of this chapter is to set out the principles (based on mechanics) that allow such questions to be addressed and to answer some of these questions.

There are two approaches to the study of fluid flow in porous media. The first is a continuum approach where average values of relevant flow properties such as porosity, permeability and tortuosity are considered. The average is taken over the smallest volume that is considered representative at each point in the system. Relatively simple models of the pore space and interconnecting channels are proposed to arrive at relations that describe the flow of fluids through the system. Such relations include Darcy's law that describes slow ("creeping") flows where inertia can be neglected, Forchheimer's equation (or, the Ergun equation) that describes faster flows where inertia becomes important and the Kozeny-

Carman law that links connected porosity to permeability. These relations are commonly quite satisfactory in many situations and are widely used. There are however many situations (and an example is the localisation of hydrothermal systems at the regional scale) where such continuum approaches are not as useful as the second, or discrete, approach.

In the discrete approach the important feature is the connectiveness and geometry of the permeable network of pores and of throats that connect the pores. As such, the approach considers the fractal geometry of the permeable network and the ways in which this geometry evolves with time. The discrete approach is based on percolation theory and proposes that the porous medium can undergo a phase transition defined by a critical probability of continuous network formation that is characteristic of the overall geometry of the system. At this critical probability the rock mass develops a continuous network of permeable fractures or other fluid pathways that allows fluid flow to occur. The continuous network is called the flow network *backbone*. This approach is ideally suited to the study of fracture networks. Since the velocity of flow through a planar fracture or of a cylindrical pore is proportional to the cube or the fourth power respectively of the aperture, the flow system is highly nonlinear and dominated by the size of the smallest restriction in that connected flow path with the largest small constriction.

We describe both the continuum and discrete approaches in this chapter but concentrate on the discrete and percolation approaches in Section 3.6.

3.1.1 Evidence for the influx of fluids.

Fyfe et al. (1978), presented a case for large scale infiltration of fluids during metasomatism. Since then a large number of studies (Dipple and Ferry, 1992; Ferry, 1994; Oliver, 1996; Ague, 2011) has supported this concept of extensive infiltration. A classification of fluid flow regimes during deformation, metamorphism and metasomatism given by Oliver (1996) highlights the range of observations. We present a slightly modified version of that classification in Figure 3.1. It differs from that of Oliver in that the presence of closed systems dominated by diffusive flow has been explicitly highlighted together with a thermal overlay which we develop throughout the remainder of this chapter.

There is no doubt that some form of fluid infiltration is necessary to promote many metamorphic reactions and in some instances metamorphic rocks have been exposed to high temperatures and pressures with no reactions taking place until H_2O (or H^+) is introduced (Austrheim, 1987; White and Clarke, 1997; Rubie, 1998; Jones and Schenk, 2003).There is still some debate as to the role of fluid flow in pore space in high grade metamorphic rocks (Yardley, 2009) or in some mylonites (Fitzgerald et al., 2006). Some (Oliver, 1996; Oliver and Ord, 1997; Ague, 2011) have emphasised that flow can be channelized so that some parts of metamorphic terrains see low fluid fluxes whilst neighbouring parts are exposed to strongly focussed flow. At high metamorphic grades where partial melting occurs, flow in leucosomes has been proposed (Brown, 2012). For some workers (Etheridge et al., 1983, 1984) the concept of thermal convection is important. Although thermal convection is said to be impossible in systems with a lithostatic fluid pressure gradient (Wood and Walther, 1986), it turns out that it is possible, in principle, in some forms of open systems with super-hydrostatic fluid pressure gradients (Zhao et al., 2008, §4.2). The question is: *What form do convective systems take in compartments with lithostatic pressure gradients and are such*

systems common or even possible under crustal conditions? We explore these concepts in §3.5.3.

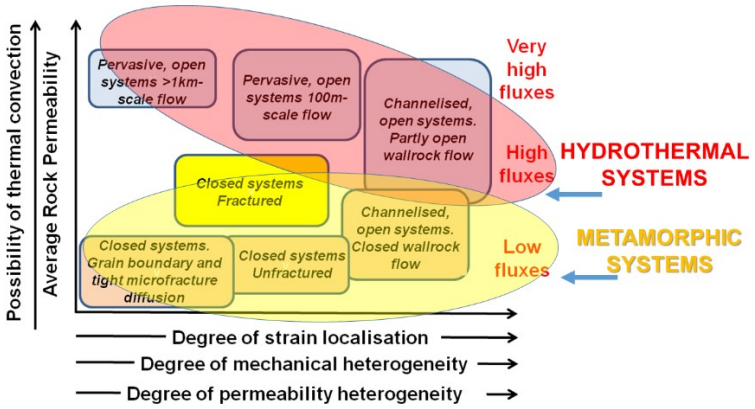

Figure 3.1. A classification of fluid flow regimes in crustal systems. The common fields for hydrothermal and metamorphic systems are shown. Modified after Oliver (1996).

In Figure 3.2 we present some examples where the influence of fluids is widely proposed. These include in particular, vein systems of various forms (Figures 3.2 a, b, c), and breccia (Figures 3.2 d).

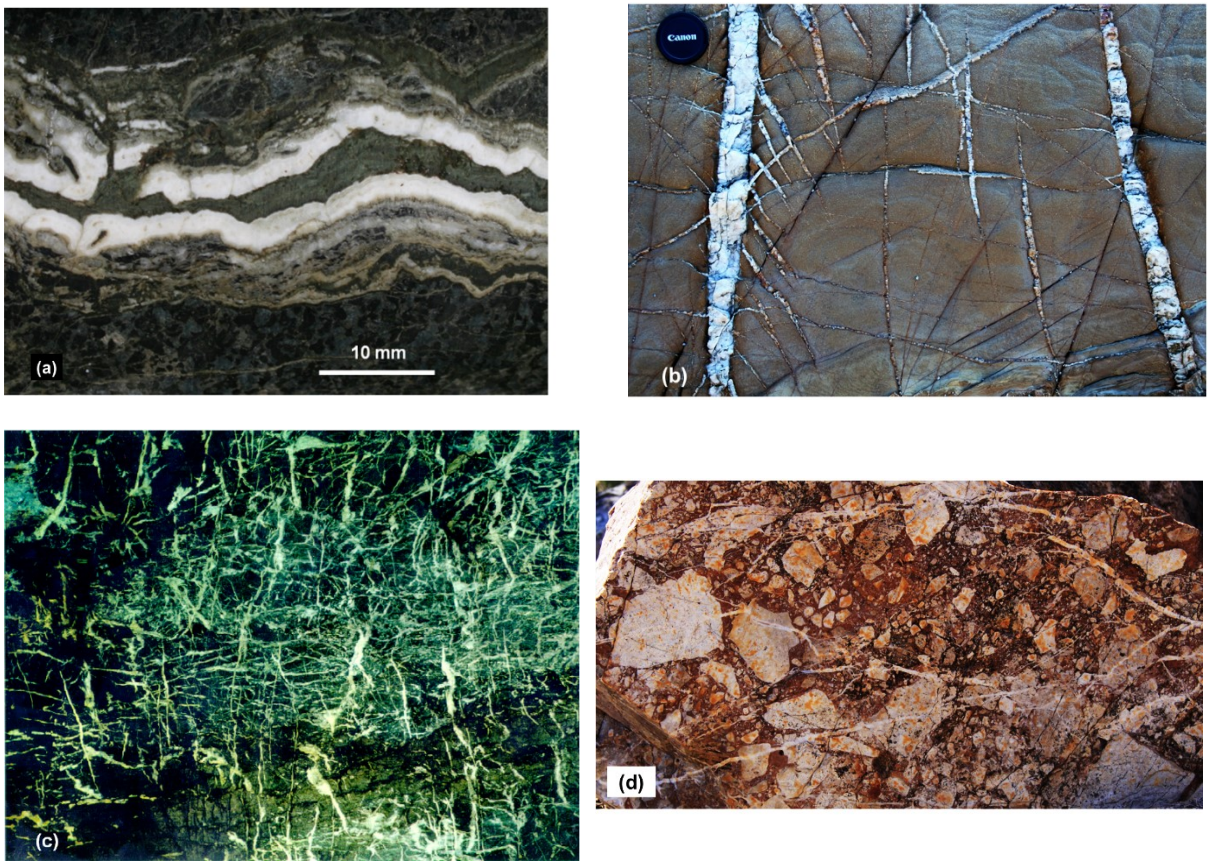

Figure 3.2. Some examples of fabrics associated with fluid flow in deforming rocks. (a) Vein system, Sirius ore body, Western Australia. (b) Vein systems in low grade greenschist turbidites, Bermagui, NSW. (c) Vein system

Hilton Mine. Mt Isa, Queensland. Image is ~ 1 m across. (d) Breccia with veining from Fountain Springs, North Queensland. Outcrop is ~ 1 m across.

Fluids associated with metasomatism arise from a number of sources including meteoric sources, connate waters, fluids released by devolatilisation (including decarbonisation, hydrocarbon release from organic material and dehydration of (OH)-bearing minerals), release of volatiles from crystallising melts, and partial melting. The chemical and isotopic characteristics of these fluids and the roles they play in metamorphic processes are discussed by Crawford and Hollister (1986) and Yardley (2009). This list does not include fluids derived from the mantle. We examine these in greater detail in Chapter 4.

3.1.2. Influence of fluids on deformation. *Effective stress.*

A detailed discussion of the coupling between deformation and fluid flow is difficult because deformation is commonly (see Hobbs and Ord, 2015) viewed from a Lagrangian point of view (the system description is in terms of some prior reference state) whereas fluid flow is viewed from an Eulerian point of view (the system description is in terms of the current state). Those interested in a rigorous integration of the two approaches should consult Coussy (1995). We consider only one aspect of the coupling here, namely, the concept of *effective stress*.

For rocks with connected pore space (including fracture networks) the concept of effective stress (Terzaghi, 1936) is commonly adopted. This concept proposes that the pore fluid pressure decreases the stress felt by the solid framework of the rock so that the deformation is controlled by an *effective stress* given by:

$$\sigma_{ij}^{effective} = \sigma_{ij} + \delta_{ij} P^{fluid} \qquad (3.1)$$

The plus sign arises because we assume compressive stresses to be negative. This principle is true only if the solid framework of the porous solid undergoes negligible volume change during deformation. Notice that P^{fluid} is not in general equal to the mean stress so that $\sigma_{ij}^{effective}$ is not in general equal to the deviatoric stress. This also means (see §3.3.3) that, in general, fluid flow is not driven by gradients in mean stress (Ridley, 1993). For discussions of the effective stress principle see Detournay and Cheng (1991), Coussy (1995, 2004, 2010), Vardoulakis and Sulem (1995, §5.3) and Paterson and Wong (2005; Chapter 7). We consider this issue further in Section 3.3.3.

The common interpretation of the effective stress principle is shown in Figure 3.3 where the yield criterion for a frictional material is shown in the absence of a pore pressure in 3.3 (a). The addition of a pore fluid pressure translates the stress σ_{ij} to $\sigma_{ij}^{effective}$ (Figure 3.3 b) as described by (3.1) and ultimately results in failure in these materials if P^{fluid} is large enough.

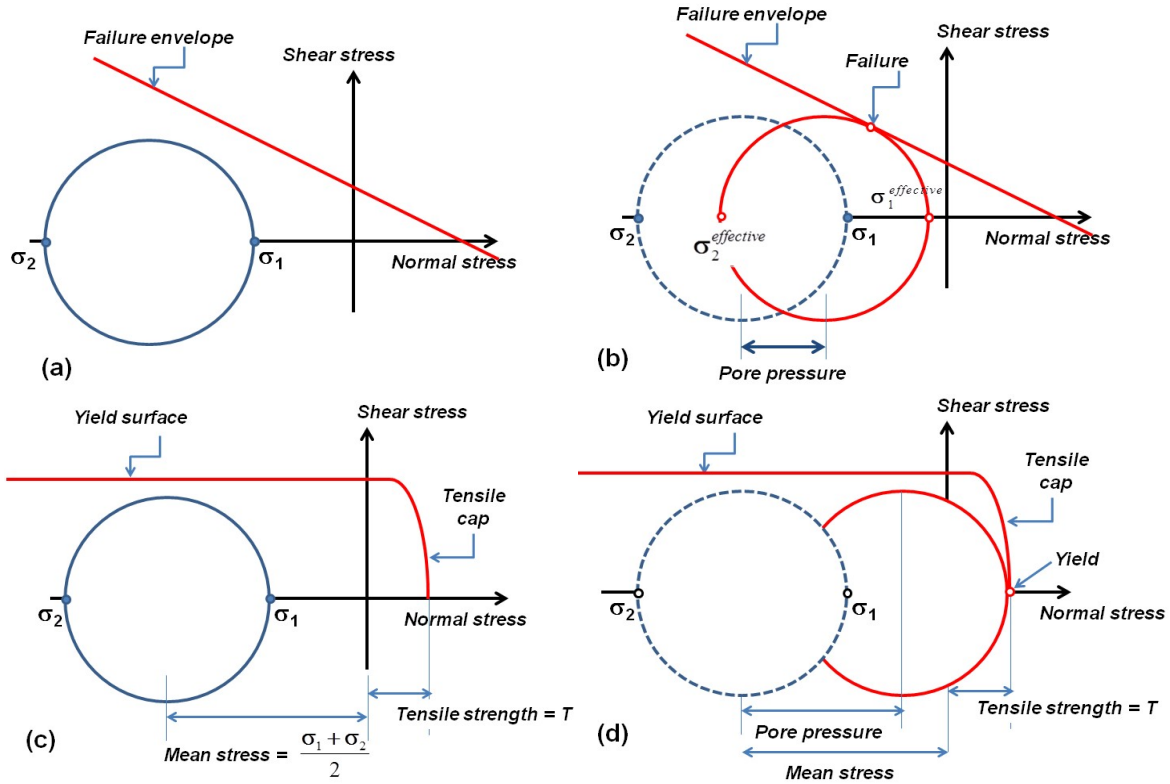

Figure 3.3. The effective stress principle applied to failure of frictional and non-frictional plastic materials. (a) A frictional porous material with a failure envelope shown in red. The imposed stress is (σ_1, σ_2) represented by the full blue circle. No fluid is present and the stress circle does not touch the failure envelope so that the stress state corresponds to elastic deformation. (b) A fluid pressure is added as indicated. This translates the initial stress state to a new effective stress state $\left(\sigma_1^{effective}, \sigma_2^{effective}\right)$ as given by (3.1). If the fluid pressure is high enough the material fails. (c) A non-frictional plastic porous material with a yield surface shown in red. A tensile cap is added to describe tensile yield at a tensile yield strength, *T*. The imposed stress is (σ_1, σ_2) represented by the full blue circle. No fluid is present and the stress circle does not touch the yield surface so that the stress state corresponds to elastic deformation. (d) A fluid pressure is added as indicated. This translates the initial stress state to a new effective stress state given by (3.1) and represented by the full red circle. If the fluid pressure is high enough the material yields at a stress state given by $\left(\frac{\sigma_1 + \sigma_2}{2} + T\right)$. However this does not imply (as shown here) that the pore pressure is equal to the mean stress.

Even though the deformation of frictional materials is commonly considered to be rate independent, the applicability of the effective stress principle to failure is dependent on the relative rates of deformation and of fluid flow. Above a critical strain-rate the effective stress principle is not a good approximation to the observed behaviour (Brace and Martin, 1968; Rutter, 1972; Paterson and Wong, 2005).

The concept of failure induced by a change in effective stress is used indiscriminately in the geosciences for any material. One should note that Figures 3.3 (a and b) apply to a frictional material such as Mohr-Coulomb or Drucker-Prager (See Hobbs and Ord, 2015). For materials where the yield surface everywhere parallels the hydrostatic axis (Figures 3.3 c and d; see Hobbs and Ord, 2015) changes in the total stress arising from an increase in pore fluid pressure initiate yield only if one postulates a *tensile yield cap* on the yield surface as shown. Although this is reasonable from a mechanical point of view, and well-studied experimentally

for brittle failure (Paterson and Wong, 20005), experimental data on tensile yield of non-frictional visco-plastic materials due to changes in effective stress are rare. Notice that in general the fluid pressure cannot equal the mean stress without initiating failure (Figure 3.3d) before that pressure is attained. Clearly (from Figure 3.3 d) such a situation is possible if the tensile strength is large compared to the shear stress in the material.

3.1.3. Hydrostatic and over-pressured fluid systems. Critical height.

It is commonly proposed that during metasomatism rocks are subjected to fluid pressures that are everywhere lithostatic; this is especially true if veins are present. The result is that the *fluid pressure gradient* is lithostatic and hence there must be an upward flow of fluid throughout the system. If the drivers for fluid influx decrease this flow tends to drive the fluid pressure gradient towards hydrostatic. When the lithostatic gradient is not maintained by the supply of new fluid the fluid pressure gradient relaxes to near hydrostatic on a time scale of $\left(H^2 / \kappa^{fluid}\right)$ where H is the height of the system and κ^{fluid} is the *fluid diffusivity* given (Phillips, 1991, p80) by:

$$\kappa^{fluid} = \frac{KV_P^2 \rho_0^{fluid}}{\mu^{fluid}\phi} \qquad (3.2)$$

where K is the permeability, V_P is the P-wave velocity in the fluid, ϕ is the porosity, ρ_0^{fluid} is the fluid density at some reference state and μ^{fluid} is the fluid viscosity. This means that although the compartment is over-pressured the fluid pressure gradient relaxes to hydrostatic. If we take the values given in Table 3.1 for water together with $V_P = 1.4 \times 10^3$ m s^{-1}, $\phi = 0.2$ and $K = 10^{-13}$ m^2 we obtain $\kappa^{fluid} \approx 1$ m^2 s^{-1}. Clearly this value depends strongly on the values of K and ϕ. For instance for a tight metamorphic rock with $K = 10^{-18}$ m^2 and $\phi = 0.01$, $\kappa^{fluid} \approx 2 \times 10^{-4}$ m^2 s^{-1}. This is still about two orders of magnitude larger than the typical thermal diffusivity for rocks (Chapter 2) of $\kappa^{thermal} \approx 10^{-6}$ m^2 s^{-1}. Thus in general *fluid pressure will diffuse through rocks faster than temperature*.

Table 3.1. Representative numerical values for various material constants and parameters for water and for rock.

Quantity	Symbol	Value
Water		
Density	ρ_0^{fluid}	1000 kg m^{-3}
Specific heat	c_P^{fluid}	4185 J kg^{-1} K^{-1}
Coefficient of thermal expansion	β_T^{fluid}	2x10^{-4} K^{-1}
Dynamic viscosity	μ^{fluid}	10^{-3} Pa s (see also Figure 3.6)
Thermal conductivity	k^{fluid}	0.6 Wm^{-1}K^{-1}
Rock		
Density	ρ_0^{solid}	2700 kg m^{-3}
Specific heat	c_P^{solid}	815 J kg^{-1} K^{-1}
Thermal conductivity	k^{solid}	3.35 Wm^{-1}K^{-1}

For the values taken for water, a value of $\kappa^{fluid} \approx 1$ m^2 s^{-1} means that a lithospheric pressure gradient in an isolated compartment 1 km high will relax to a hydrostatic pressure gradient on a time scale of 10^6 seconds or about 11 days. A value of $\kappa^{fluid} \approx 2 \times 10^{-4}$ m^2 s^{-1} increases the relaxation time in this chamber to 160 years. This relaxation in fluid pressure gradient produces compressive stresses at the base of the compartment and effective tensile stresses at the top as discussed by Zhao et al. (2008). The maximum height, $H^{critical}$ (Figure 3.4) of a body of rock that can support a given fluid pressure gradient is:

$$H^{critical} = \frac{\overline{\sigma}^{compressive} + \overline{\sigma}^{tensile}}{\left(\rho^{rock} - \alpha\rho^{fluid}\right)g} \qquad (3.3)$$

where $\overline{\sigma}^{compressive}$ and $\overline{\sigma}^{tensile}$ are the compressive and tensile strengths of the rock and α is a factor that measures how far the fluid pressure gradient is above hydrostatic; $\alpha = 1$ for a hydrostatic fluid pressure and $\alpha = 2.7$ for a lihostatic fluid pressure gradient with an average rock density of $\rho^{rock} = 2700$ kg m^{-3}. Thus if $\left(\overline{\sigma}^{compressive} + \overline{\sigma}^{tensile}\right) = 50$ MPa, say, then $H^{critical} =$ 3 km for a hydrostatic fluid pressure gradient. If the height of the hydrostatically pressured compartment is greater than $H^{critical}$ then the pore space at the base collapses and the top localises in the form of fractures in a manner considered by Connolly and Podladchikov (1998) for the generation of porosity waves.

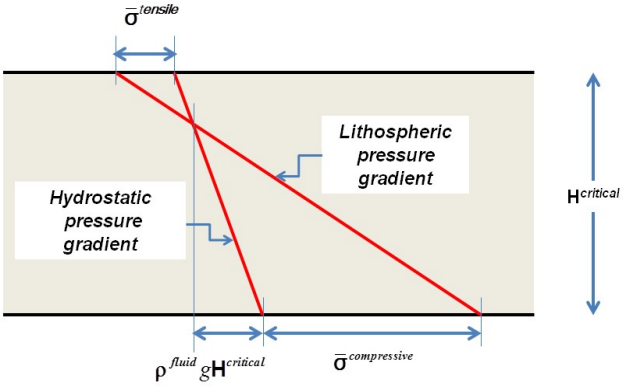

Figure 3.4. The critical height for a hydrostatic fluid pressure gradient.

Although we have framed the argument above in terms of a system where an initial lithospheric pressure gradient is relaxed following the closure of the fluid supply, an identical argument applies to a layered crustal system where a low permeability lithostatically pressured system is overlain by a layer with higher permeability. We will see (§3.2.3) that the high permeability layer must have a fluid pressure gradient that is below lithostatic and its thickness is then controlled by (3.3).

3.2. Types of fluid flow.

Flow in metamorphic systems takes place at small spatial scales within nano-films or channels on grain boundaries up to the scale of kilometres in fluidised hydrothermal breccias (Figure 3.5 a). Within this wide range of spatial scales, a wide range of mechanisms is involved in the transport of fluid phases. At the scale of grain interfaces, or closed micro-cracks within grains, transport is presumably by diffusion. At a slightly larger length scale there is a transition between what one would normally call *diffusion mechanisms* and *flow in nano- to micro-pore structures*. This is the regime where flow in the pore structures

recognised by workers such as Mancktelow et al. (1998), Mancktelow and Pennacchioni (2004) and Putnis (2009) is relevant. At the nano-scale, flow is not described by the *Navier-Stokes equations* (Hughes and Brighton, 1999) which are the classical equations that describe the flow of linear fluids under the influence of a pressure gradient and is better described by the *Burnett equations* (Roy et al., 2003).

As one increases the length scale, there is a transition to where the Navier-Stokes equations can be used but the fluid does not stick to the walls of the flow channel; at larger length scales the fluid does stick to the walls. At the next scale up, fluids in grain boundaries and closed fractures can aggregate to form bubbles and the bubbles can diffuse. At the next scale, assuming that the fluid is Newtonian viscous, the transport process is described by the *Navier-Stokes equations* (Hughes and Brighton, 1999) and the fluids can be assumed to stick to the walls of the flow channel. This is the scale where Darcy's law begins to be applicable. At the scale where fluid transport can be considered to take place in open fractures, as is the case in many hydrothermal and breccia systems, the flow is described by Navier-Stokes equations although it may be possible in some situations (where the flow is slow enough) to describe flow through a large enough volume in terms of Darcy's law.

In Chapter 7 we point out that the complex topology of three dimensional fluid filled porous networks leads to fluid stretching and folding within the flow channels and hence *chaotic advection* (Ottino, 1989, 1990; Metcalfe, 2010; Lester et al., 2012). This is an important process for enhancing both fluid mixing and the rates of chemical reactions (Tel et al., 2005). At the scale where a porous solid can be considered homogeneous with respect to pore distribution, the chaotic advection within pores can be averaged (Phillips, 1991) so that the flow (as long as it is slow enough) is represented, macroscopically, by *Darcy's law*.

Chaotic advection is possible from the smallest to the largest scales in open pore and fracture networks so long as the networks are three dimensional and produce a flow geometry that branches and merges (Lester et al., 2012). If the fluid velocity is large enough for a given length scale, the flow becomes *turbulent*. This is the case in some hydrothermal systems (Figure 3.5 b). It is important to note that *chaotic advection* is different to *turbulent flow* of fluids; chaotic advection can occur in a laminar flow (Metcalfe, 2010). In non-turbulent chaotic flows the Eulerian description of the flow at any instant is laminar however the flow is unsteady so that the history of the Lagrangian description is chaotic. For turbulent flows the Eulerian description of the flow at any instant is not laminar and the streamlines define a cascade of dissipative structures over many length scales. Chaotic mixing can occur for both unsteady laminar flows and turbulent flows (Ottino, 1990; Metcalfe, 2010).

Some distinctions between various flows and examples in the geosciences are shown in Figure 3.5 (a). We discuss these various processes throughout the remainder of this chapter but first we need some tools that enable us to describe the nature and geometry of these various flows and the ways in which they transport heat, dissipate energy and promote chemical reactions (Figure 3.5 b, c).

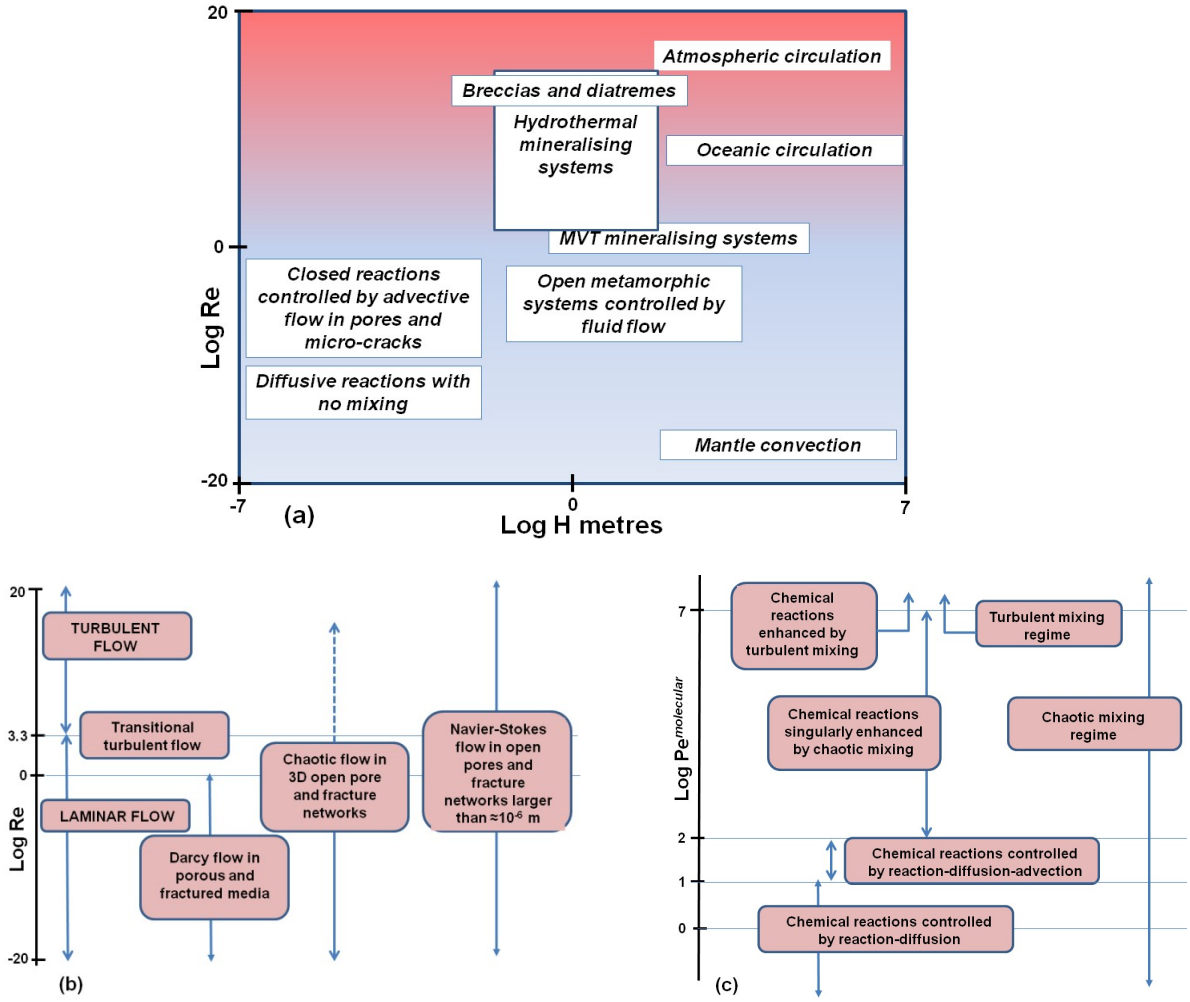

Figure 3.5. Characteristics and examples of various kinds of fluid flows. (a) Positions, within spatial scale – Reynolds number space, of various kinds of flow processes in the geosciences. The positions are diagrammatic and not meant to represent conditions precisely. Motivated by Ottino (1990) and Metcalfe (2010). (b), (c) Distinctions between various kinds of flows based on the Reynolds number and Peclet number related to molecular diffusion.

3.2.1 The dimensionless groups: The Knudsen number, the Reynolds number, the Peclet numbers and the Rayleigh numbers.

Dimensionless numbers of various kinds are useful in discussing the flow of fluids in a range of environments. Four of these dimensionless numbers are the Knudsen number, Kn, the Reynolds number, Re, the Peclet number, Pe, which can be defined both for molecular diffusion, $Pe^{molecular}$ and the diffusion of heat, $Pe^{thermal}$, and the Rayleigh number which can be defined for both temperature boundary conditions, Ra^{T}, and for fluid flux boundary conditions, Ra^{flux}. These are defined below.

The Knudsen number, Kn, is a number useful in defining the lower limit in length scale where the Navier-Stokes equations are relevant and the transitions to other forms of transport in micron to nanometre scale flow channels. Kn is defined as the ratio of the mean-free-path, π, of molecules and the macroscopic length scale of the pore space, Π:

$$\mathrm{Kn} = \frac{Mean\text{-}free\text{-}path\ of\ molecules}{Length\ scale\ of\ pores} = \frac{\pi}{\Pi}$$

For Kn > 10^{-1} the Navier-Stokes equations cease to be relevant in describing the flow.

The *Reynolds number* is the ratio of inertial forces to viscous forces in a flow:

$$\mathrm{Re} = \frac{Inertial\ forces}{Viscous\ forces} = \frac{Total\ momentum\ transfer}{Molecular\ momentum\ transfer}$$

Or,

$$\mathrm{Re} = \frac{\mathrm{H}\rho_0^{fluid}}{\mu^{fluid}} v \qquad (3.4)$$

where H is a characteristic length for the system in the direction of flow, v is the physical velocity of the fluid, ρ_0^{fluid} is the density of the fluid in some reference state and μ^{fluid} is the fluid viscosity (units: Pa s). If flow is slow and within the pores of a porous solid, v is given by:

$$v = \hat{\mathrm{V}} / \phi \qquad (3.5)$$

where $\hat{\mathrm{V}}$ is the Darcy velocity (units: $m^3\ m^{-2}\ s^{-1}$; see §3.2.3 and Figure 3.7) and ϕ is the porosity. For porous flow in metamorphic rocks typical values are $\hat{\mathrm{V}} = 1\ \mathrm{m\ y^{-1}}$ (or less), ϕ = 0.05, H = 10^{-3} m, and μ^{fluid} = 10^{-4} Pa s. Thus, Re ≈ 6 x 10^{-3} which means viscous forces dominate. Low Reynolds numbers are typical of fluid flow in many metamorphic systems.

The condition Re < 1 is necessary for Darcy's law to hold (see §3.2.3; Phillips, 1991, p 28). For Re < 1 the flow is laminar which means that in a simple shearing flow the fluid particles move in parallel planes. For these conditions the effect of fluid advection upon mixing is negligible; any chemical reactions that take place in the fluid occur by diffusion across interfaces between different fluids and hence are very slow. Above the threshold Pe = 10^2 (if the flow is chaotic; figure 3.5 c) mixing rates and chemical reactions are enhanced by several orders of magnitude (Tel et al., 2005) although for such flows Darcy's law is no longer applicable. Chemical reactions are enhanced by turbulent mixing above Pe = 10^7 (Villermaux, 2012). We revisit this issue in §3.2.5. Oliver et al. (2006) calculate fluid velocities greater than 1 m s^{-1} in a breccia system from Cloncurry, Australia, with length scales up to 1 km. Assuming the values given in Table 3.1 for water, the Reynolds number is of the order of 10^{10}. This is an extreme value and one could expect strong turbulent mixing with greatly enhanced chemical reaction rates. The point is that although the value of the Reynolds number is commonly less than 1 in metamorphic systems there are examples, particularly in hydrothermal breccia systems, where values greater than 10^7 exist. Under such conditions Darcy's law is no longer applicable and the Ergen equation or some related expression describes the flow.

For fluid flows that transport mass and heat the *Peclet number* is the ratio of the time scale for molecular diffusion, or the diffusion of heat, to the time scale for advection in a flow:

$$\mathrm{Pe} = \frac{Time\ scale\ for\ diffusion}{Time\ scale\ for\ advection}$$

In particular, for Darcy flow coupled to the diffusion of heat or mass,

$$\mathrm{Pe}^{thermal} = \frac{\mathrm{H}\rho_0^{fluid} c_P}{k_e} \hat{\mathrm{V}} \quad \text{and} \quad \mathrm{Pe}^{molecular} = \frac{\mathrm{H}}{D} \hat{\mathrm{V}} \qquad (3.6)$$

where H is a length scale for the system in the direction of flow, ρ_0^{fluid} is the reference density of the fluid, c_P is the specific heat of the fluid, $\hat{V}$ is the Darcy velocity (related to the physical fluid velocity by (3.5)) and k_e is the effective thermal conductivity of the fluid saturated solid given by

$$k_e = \phi k^{fluid} + (1-\phi) k^{solid}$$

k^{fluid} and k^{solid} are the thermal conductivities of the fluid and unsaturated solid respectively. D is the molecular diffusivity. Taking the values for water given in Table 3.1 and assuming ϕ = 0.1 then k_e =3.08 W m^{-1} K^{-1}. We assume this value in future calculations in this chapter.

If $\hat{V}$ =1 m y^{-1} then, given the values of ρ_0^{fluid} and c_P for water in Table 3.1 and taking k_e = 3.08 W m^{-1} K^{-1}, we obtain $Pe^{thermal}$ = 43 for H = 1 km. Phillips (1991, pp 213-216) gives examples of $Pe^{thermal}$ = 300 for flows in sedimentary basins and of how such large values influence the possible temperature distributions in such basins and hence the localisation of MVT deposits in such basins. We will see later in this chapter that in metamorphic systems with a lithostatic fluid pressure gradient, thermal Peclet numbers greater than about 1 are unlikely unless large scale advection of heat dominates the system as in some large hydrothermal systems.

The *Rayleigh number* is the ratio of the buoyancy forces to the viscous forces in a fluid:

$$\mathrm{Ra} = \frac{Buoyancy\ forces}{Viscosity\ forces}$$

For a system with given boundary conditions and geometry a value for a *critical Rayleigh number* exists that marks the transition from pure conduction to fluid convection as the mode of heat transfer. This value of Ra is known as a *critical Rayleigh number,* $\mathrm{Ra}_{critical}$, for that system. The boundary conditions for a system with a given geometry consist of various combinations of fixed temperature, fixed heat flux, fixed fluid pressure and fixed fluid flux. Examples of values of $\mathrm{Ra}_{critical}$ for 10 different sets of boundary conditions are given by Nield and Bejan (2013, Table 6.1). As the temperature gradient or heat supply to a given system is increased the convection pattern commonly undergoes transitions to new modes of behaviour at new critical Rayleigh numbers. These transitions include switches to new wavelengths and patterns of convection including oscillatory and chaotic behaviour (Nield and Bejan, 2013, §6.8).

Thus the precise form of the Rayleigh number depends on the boundary conditions for the problem. If the boundary conditions are fixed temperatures, T and T_0 respectively, at the base and top of the compartment (corresponding to the classical Horton-Rogers-Lapwood view of a convecting system; Nield and Bejan, 2013, Chapter 6) then the relevant Rayleigh number is:

$$\mathrm{Ra}^{\mathrm{T}} = \frac{(\rho_0^{fluid} c_P)\rho^{fluid} g \beta_T^{fluid} (\Delta T) K H}{\mu^{fluid} k_e} \qquad (3.7)$$

where

$$\rho^{fluid} = \rho_0^{fluid}\left[1 - \beta_T^{fluid}\left(T - T_0\right)\right], \qquad (3.8)$$

and $\Delta T = T - T_0$ is the temperature difference between the top and bottom of the compartment. β_T^{fluid} is the coefficient of thermal expansion of the fluid.

If on the other hand the boundary conditions comprise applied thermal and fluid fluxes at the base of the system and fixed temperature and fluid pressure at the top, then the relevant Rayleigh number is:

$$Ra^{flux} = \frac{(\rho_0^{fluid} c_P)\rho^{fluid} g\beta_T^{fluid} qKH^2}{\mu^{fluid} k_e^2} \qquad (3.9)$$

where q is the heat flux imposed at the base of the system. This corresponds to the situation in most metamorphic/hydrothermal systems. Given the values for water in Table 3.1 and assuming $\phi = 0.1$ then numerically,

$$Pe^{thermal} = 1.359x10^6 H\hat{V} \qquad (3.10)$$

$$Ra^T = 2.66x10^9 (\Delta T)KH \qquad (3.11)$$

$$Ra^{flux} = 8.82x10^8 qKH^2 \qquad (3.12)$$

As examples, if H = 1 km and $\hat{V}$ is 10 mm y^{-1} then $Pe^{thermal}$ =0.43. Ra^T is 79.8 for a temperature difference between the top and bottom of 300°C and a permeability of 10^{-13} m^2. For H = 10 km, a basal heat flux of 60 mWm^{-2}, a lithostatic fluid pressure gradient and K = 10^{-18} m^2, $Pe^{thermal}$ = 2.3 and Ra^{flux} = 5.3.

Note that the viscosity of water decreases rapidly with increasing temperature (Figure 3.6) at crustal pressures in the range 0 °C to ~700 °C (Abramson, 2007); the variation in viscosity, μ^{fluid}, with temperature is given approximately by $\mu^{fluid} = A[10^{B/(T-C)}]$ where A = 2.414×10^{-5} Pa s, B = 247.8 K and C = 140 K. For temperatures greater than about 300°C the viscosity of water is about 10^{-4} Pa s.

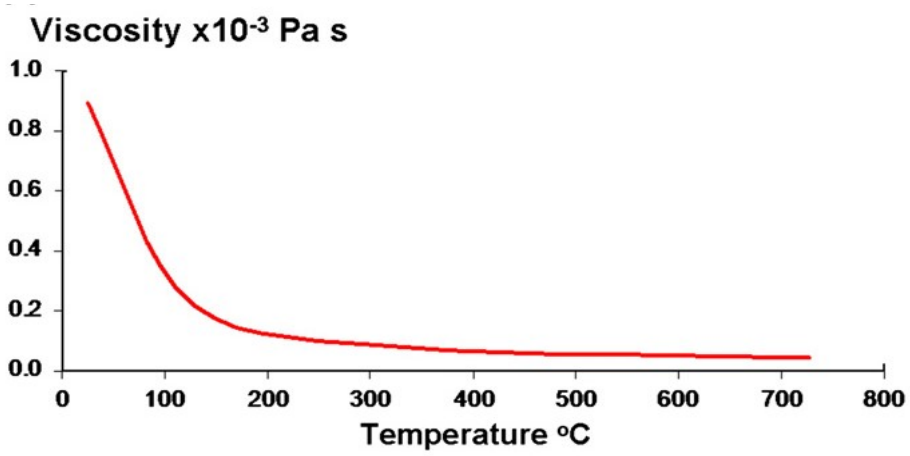

Figure 3.6. Variation of the viscosity of pure water with temperature.

3.2.2. Grain boundary and micro-fracture flow.

Transport of fluids in metasomatic rocks takes place at a number of scales ranging from the grain scale, in the case of reacting metasomatic rocks at high pressures, or deformation by pressure solution, to flow in open cracks both within grains and at coarser scales (Etheridge et al., 1983, 1984). In hydrothermal systems, particularly in hydrothermal breccias, flow may be in open fractures and take place on the kilometre-scale.

The detailed mechanism (or mechanisms) of transport of fluids in metasomatic rocks remains a matter of speculation although several models have been proposed that are worthy contenders. As Etheridge et al. (1983) point out, the initial porosity that is present in un-metamorphosed rocks is modified and probably largely obliterated by chemical reactions and

grain boundary adjustments during metamorphism to produce a *metamorphic porosity* that comprises planar films on grain boundaries, pores ("bubbles" or "voids") along grain boundaries (White and White, 1981; Mancktelow et al., 1998; Mancktelow and Pennacchioni, 2004; Billia et al., 2013), channels or tubes along the boundaries between three grains (Hay and Evans, 1988), and nano-porosity generated by dissolution processes (Putnis, 2009). In addition, Etheridge et al. (1983) proposed a *fracture porosity* that is envisaged to develop by hydrofracturing at the grain scale (Etheridge et al., 1984; Cox and Etheridge, 1989). We discuss below porosity structure and generation, and hence permeability, at the grain scale.

The evolving grain boundary structure. The nature of grain boundaries is important not only for controlling the transport of fluids but for the mechanical behaviour of a polycrystalline aggregate during deformation. Thus Paterson (1995) distinguished three different models for fluid transport in grain boundaries in the context of fluid assisted granular flow and showed that each results in a different dependence of the flow stress upon the grain-size and/or other parameters such as the porosity or molar volume. Thus the details of grain boundary structure and the ways in which fluids are incorporated into that structure have wide implications not only for fluid transport mechanisms but for the mechanical response during deformation and for the mechanisms of metasomatic reactions.

Micro-cracking. Micro-cracking processes are by far the most dramatic ways of changing permeability. The actual increase in permeability produced by arrays of cracks and/or tubes depends on the precise geometry and statistics of the defects but a feeling for the effect can be gained by considering an array of parallel cracks with apertures δ. The permeability arising from arrays of parallel cracks which generate a porosity, ϕ, is $\approx 10^{-2}\phi\delta^2$ (Phillips, 1991, pp 29-34). An array of micro-cracks with an average number of cracks per unit area of ε gives a porosity $\phi = \delta\varepsilon$ and so (assuming all the new porosity is connected) the permeability is $\approx 10^{-2}\varepsilon\delta^3$. Thus if $\delta = 10^{-5}$ m and $\varepsilon = 10^3$ m^{-2} then the permeability is $\approx 10^{-14}$ m^2. If the rock initially had a permeability below the percolation limit (say 10^{-22} m^2) then this micro-cracking represents a very substantial increase in permeability.

These kinds of arguments are supported experimentally. Micro-cracking induces a permeability increase that can be quite dramatic (Fredrich and Wong, 1986). Near the percolation threshold a number of workers (see Meredith et al., 2012 for a review) have proposed a relation:

$$K = K_0 \left(\phi - \phi_c\right)^n$$

where K is the permeability (in m^2), ϕ is the total porosity (expressed as a %) and ϕ_c is the percolation threshold for fluid flow; K_0 is a characteristic permeability when $\phi - \phi_c$ is 1%. *n* is a critical parameter to be determined by experiment but values in the range 2.3 to 3.8 have been reported (Meredith et al., 2013). The experiments of Meredith et al. (2013) demonstrate a permeability increase from less than 10^{-22} m^2 with a porosity of 1% increasing to about 10^{-16} m^2 at a porosity of 5%. This change in permeability has been proposed on the basis of percolation theory by Berkowitz and Balberg (1992) and Feng et al. (1987). This means, as suggested by Etheridge et al. (1983), that metamorphic rocks that are considered to be of very low permeability by writers such as Yardley (2009) and Connolly (2010) can become highly permeable with just the slightest amount of micro-cracking.

Reaction induced porosity. Many authors have proposed that permeability can be generated directly by hydrothermal reactions. The mechanisms involve a spectrum of behaviours that range from an influence of released fluid or melt pressure on the effective stress thus inducing fracture (Connolly et al., 1997) to volume changes associated with the chemical reactions: positive ΔV reactions are proposed to generate local stresses that initiate fracture (Watt et al., 2000) and negative ΔV reactions generate local porosity decreases directly. For instance Rushmer (2000) describes situations where partial melting involving biotite (zero or small positive ΔV) results in local trapping of partial melt whereas partial melting of muscovite (large positive ΔV) results in escape of partial melts.

An important part of this spectrum of behaviour involves the mechanisms by which mineral reactions take place. The issue is strongly linked to the observation that many metamorphic reactions such as kyanite replacing andalusite, serpentinite replacing olivine or albite replacing K-feldspar, are pseudomorphic (see Vernon, 2004, §4.13.3). Pseudomrphic reactions are the norm in hydrothermal systems, a point that distinguishes hydrothermal processes from many metamorphic processes. Pseudomorphic reactions are classically considered, by definition, to be constant volume replacements even though the molar volumes of the initial and replaced phases may be quite different. One view of this process is presented by Merino and Canals (2011) who propose that the replacement process involves atom for atom displacements driven by a pressure solution process; the process does not involve solution and precipitation. Stresses are generated during this process (Fletcher and Merino, 2001) that drive pressure solution, fracture and vein formation. These stress induced fractures that are then responsible for increases in permeability.

A second view of mineral reactions (particularly those that involve pseudomorphism) derives from the work of Putnis and others (Putnis, 2009; Putnis and John, 2010) where a solution-dissolution assisted phase transition is proposed whereby solutions dissolve the parent grain to form a network of nano-metre pores and/tubes and the new replacement mineral is precipitated in these pores. It is this nano-porous network that is capable of increasing the local permeability but stress induced fracturing may be important also (Putnis, 2009).

The subject is in its infancy and an exciting future in this area is developing. The issue is important not only for models of porosity and permeability development during hydrothermal reactions, it has relevance as to how chemical reactions are written for hydrothermal systems; *should the reaction be written in terms of constant pressure (as is the classical approach) or in terms of constant volume (Lindgren, 1912; Putnis, 2009; Merino and Canals, 2011)?*

In summary: It appears that there is a complete spectrum of behaviour with respect to mechanisms of fluid transport during deformation and metasomatism. At the finest of intergranular scales or within tight microcracks the fluid comprises a nano-film. Transport is probably described by Fick's law. At a coarser scale interfaces are sites for nano-pores derived largely by chemical reactions including dissolution. As the scale increases and the pores become larger (perhaps the micron-scale) the flow can be described by the Navier-Stokes equations but with slip at the solid interface. Increasing the scale further leads to non-slip conditions at the interface and a transition to true Darcy flow. At larger scales again, in

open fractures, Navier-Stokes flow describes laminar flow. Ultimately at large Reynolds numbers, such as in breccias, the flow becomes turbulent. Chaotic flow leading to enhanced mixing is possible in all regimes where the flow at each instant can be described as laminar. Enhancement of chemical reactions takes place in these flows for Pe > 10^2. Chemical reaction enhancement by chaotic mixing is overwhelmed by turbulent mixing for Pe > 10^7. For further discussion of fluid mixing see Chapter 7.

3.2.3. Darcy flow; Porosity and Permeability.

Slow fluid flow through porous media with coordinates (x, y), with x horizontal and y vertical (positive down), is well described by *Darcy's law* which simply says that in the absence of gravity the fluid flux is proportional to the pore fluid pressure gradient. In two dimensions with gravity Darcy's law is expressed as:

$$\hat{V}_x = \frac{K}{\mu^{fluid}}\left(-\frac{\partial P^{fluid}}{\partial x}\right) \tag{3.13}$$

$$\hat{V}_y = -\frac{K}{\mu^{fluid}}\frac{\partial}{\partial y}\left(P^{fluid} - \rho^{fluid} g y\right) = \frac{K}{\mu^{fluid}}\left(-\frac{\partial P^{fluid}}{\partial y} + \rho^{fluid} g\right) \tag{3.14}$$

where $\hat{V}_x$, $\hat{V}_y$ are the horizontal and vertical components of the *Darcy fluid velocity*. These relations for Darcy's law are true for Re < 1, Kn < ≈10^{-3}, and for linear viscous fluids (Phillips, 1991).

The *Darcy velocity* is the *volume of fluid* that passes through a unit area of the material in unit time and thus has the units: [m^3 m^{-2} s^{-1}] or [m s^{-1}]. Thus although $\hat{\mathbf{V}}$ has the units of velocity, one should always remember that it represents a *volume of fluid flowing through a unit area* (Figure 3.7). The concept of the Darcy fluid velocity as a *flux* is fundamental in examining open flow systems. We loosely refer to the *Darcy flux* as the Darcy velocity.

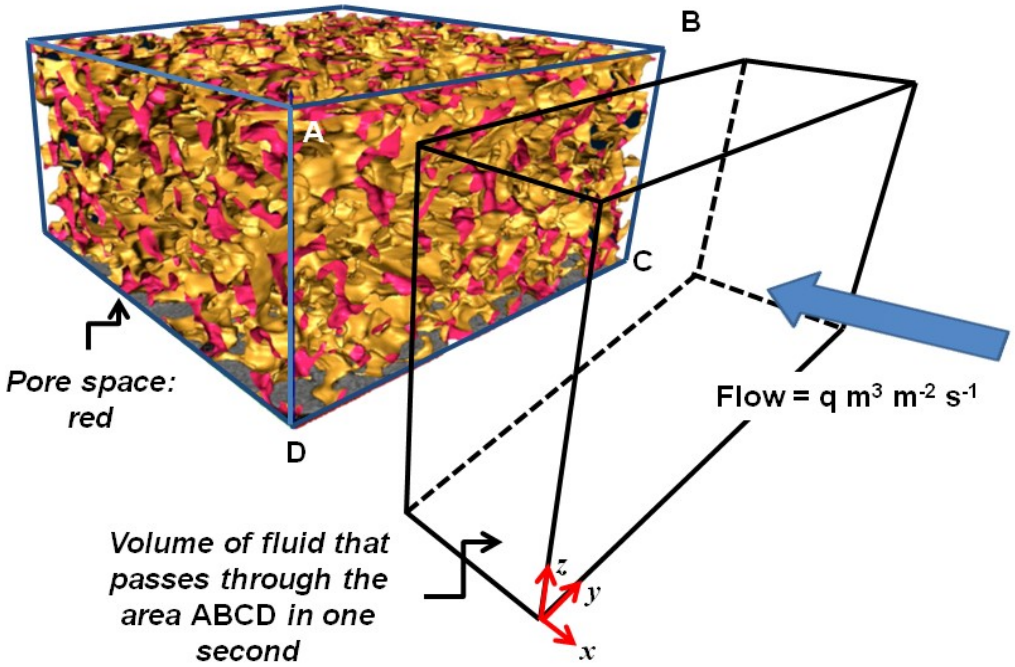

Figure 3.7. The definition of Darcy velocity. In this case the *x*-component of the Darcy velocity, $\hat{\mathrm{V}}_x$ (which for this flow is negative), is the volume of fluid that passes through the area, ABCD, of the porous solid in a second. The crimson areas represent open porosity.The image of the porous solid is supplied by Jie Liu.

In (3.13) and (3.14), K is a material quantity known as the *permeability* (with units m^2) and μ^{fluid} is the fluid viscosity (with units Pa s). P^{fluid} is the fluid pressure, ρ^{fluid} is the fluid density and g is the acceleration due to gravity. The negative sign in these equations means the fluid flows down the gradient indicated. Notice that the flow in the presence of a gravity field is not down a gradient in fluid pressure. The flow is controlled by gradients in what is variously known as the *hydraulic head,* $\mathcal{H}$, or sometimes as the *hydraulic potential*, a concept introduced by Hubbert (1940). $\mathcal{H}$ in this case is given by

$$\mathcal{H} = \left(\mathrm{P}^{fluid} + \rho^{fluid} \mathrm{g}y\right) \qquad (3.15)$$

where the coordinate *y* can be considered as the height above (or below) an arbitrary datum. The use of the term *hydraulic potential* for $\mathcal{H}$ is useful only for isothermal flows. If thermal effects are present ρ^{fluid} becomes a function of position within the thermal field and $\mathcal{H}$ ceases to be a potential for the flow.

In addition, another equation is required to express the *continuity of flow* in two dimensions. The general form of this equation is (Phillips, 1991):

$$\frac{\partial\left(\phi\rho^{fluid}\right)}{\partial t} + \nabla\cdot\left(\rho^{fluid}\hat{\mathrm{V}}\right) = Q_s$$

where Q_s is a source term with units mass per unit volume per second. If we consider systems where fluid is not generated within the system, the source term is zero. In addition, for constant porosity and fluid density we have for continuity in two dimensions:

$$\frac{\partial\hat{\mathrm{V}}_x}{\partial x} + \frac{\partial\hat{\mathrm{V}}_y}{\partial y} = 0 \qquad (3.16)$$

We will use this form of the continuity equation frequently in what follows.

The fact that fluid flow in the presence of a gravity field is not driven by gradients in fluid pressure (in general) is illustrated in Figure 3.8 where manometers are inserted in a fluid flow system in which fluid flows from a reservoir at A at constant height above a datum X-Y to another reservoir at E at a lower height so that $\mathcal{H}_\mathrm{A} > \mathcal{H}_\mathrm{E}$. The fluid flows continuously from A to E under the influence of the gradient in $\mathcal{H}$. Notice that the fluid flows from C to D even though the fluid pressure at C as measured by the height of fluid in the manometer at C, is smaller than the fluid pressure at D so that over the path C-D the fluid is flowing *up* a fluid pressure gradient (see Mandl, 1998, Figure II, 10-1).

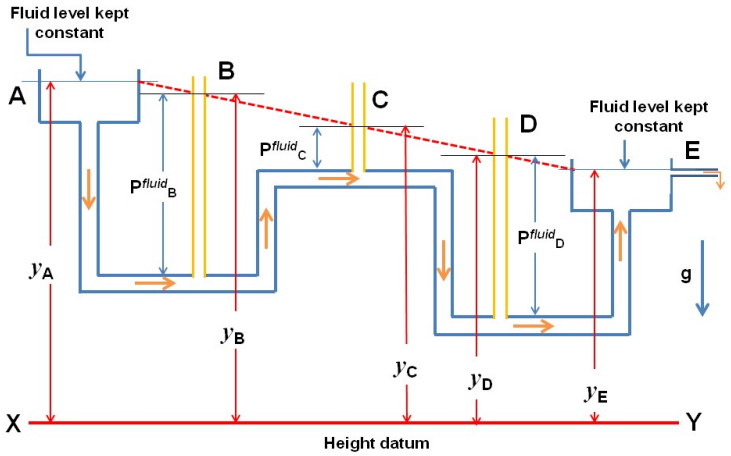

Figure 3.8. The concept of hydraulic head in the presence of a gravity field. Fluid resevoirs at A and E are kept at constant levels of fluid, y_A and y_E, above a height datum X-Y shown in red. The reservoirs are connected by a pipe shown in blue passing through the localities B, C and D. At these localities manometers record the fluid pressure shown as P^{fluid}_B, P^{fluid}_C and P^{fluid}_D. The fluid flows from high fluid pressure at B to low fluid pressure at C and then to a higher fluid pressure at D. Thus in this case fluid flows from low fluid pressure to higher fluid pressure. The fluid flow is driven by the overall gradient in hydraulic head shown by the dotted red line and not by local differences in fluid pressure. Notice that $\mathcal{H}_A > \mathcal{H}_B > \mathcal{H}_C > \mathcal{H}_D > \mathcal{H}_E$ where the hydraulic head $\mathcal{H}$ is given by (3.15).

The essential problem in applying Darcy's law to geological problems is obtaining knowledge of the permeability and its spatial distribution. As shown in Table 3.2 the permeability varies by many orders of magnitude between un-cemented sands, sandstones and "tight" metamorphic rocks with no fractures. In general the permeability for a given rock type increases with depth (See Lyubetskaya and Ague, 2009, p1511, for a discussion).

Table 3.2. Representative permeabilities of various rock types.

Rock type	Permeability m^2
Gravels and sands	10^{-9} to 10^{-12}
Shales	10^{-12} to 10^{-25}
Sandstones	10^{-11} to 10^{-17}
Limestones	10^{-12} to 10^{-16}
Marble	10^{-16} to 10^{-19}
Granites, gneisses, basalts	10^{-16} to 10^{-20}

The remaining parameter of importance in the flow of fluids through rocks is the *porosity*, ϕ, which is the ratio of the volume of open pore space to the total volume of the rock. The pore space may comprise the network of pores between individual grains or of fractures in the rock mass. If both pores between grains and fractures are present one talks of *double porosity*. Typically ϕ varies from perhaps 0.3 in un-cemented sandstones to 0.01 or less in metamorphic rocks. Since the open pore space need not be interconnected (there may be many dead end or enclosed spaces) there is no simple relationship between porosity and permeability. The subject is discussed by Walder and Nur (1984). An empirical relation known as the *Kozeny-Carman relation* which relates the porosity of a packing of regular spheres to the permeability of the array is commonly used:

$$K = K_0 \frac{\phi^3}{1-\phi^2} \qquad (3.17)$$

where K_0 is a reference permeability that depends on a reference porosity ϕ_0.

Fast fluid flows and brecciation/fluidisation.

Darcy's law is derived (Phillips, 1991) for slow linearly viscous flows (Re < 1) where the dissipation arising from momentum transfer is negligible. At higher velocities inertial effects become important and dissipation from these effects cannot be neglected. This is particularly important for fluid flow through breccias and in particular when the fluid flow is sufficiently strong to be able to lift or move individual fragments of rock, a process known as *fluidisation*. At such fluid velocities the relation between fluid pressure gradient ∇P^{fluid} and fluid velocity, *v*, is no longer linear, as in Darcy's law, but includes a term with the fluid velocity squared, expressing the increased dissipation arising from transport of momentum:

$$\nabla P^{fluid} = av + bv^2 \qquad (3.18)$$

Various forms of this equation are known as the *Ergun* and the *Wen and Yu equations* and are discussed by Niven (2002) and Bird et al. (1960). These equations were used by Oliver et al. (2006) in a study of breccia formation and transport.

Pressure distribution in a layered crust.

Most models of the crust admit of a permeability change with depth whether it be due to compaction with depth (Bethke, 1985), a transition to lower permeability metamorphic rocks (Manning and Ingebritson, 1999; Lyubetskaya and Ague, 2009)) or the presence of relatively impermeable "caps" or "seals" at mid-crustal depths (Etheridge et al., 1983). Here we explore the effects of such permeability changes on a metasomatic system where fluid is generated at depth in the crust or is introduced into the crust from the mantle.

We first consider a homogeneous crust (Figure 3.9 a). The fluid flow is specified directly by (3.13) and (3.14). If the vertical fluid pressure gradient is hydrostatic, that is, $\frac{\partial P^{fluid}}{\partial y} = g\rho^{fluid}$ then there is no flow. If the fluid pore pressure gradient is greater than hydrostatic the flow is upwards and if the gradient is less than hydrostatic, the flow is downwards. Lyubetskaya and Ague (2009, Figure 3d) give an example of downward flow driven by retrograde metamorphic reactions at depth. This same downward flow can result from alteration mineral reactions that convert anhydrous silicates to hydrous ones (see Chapter 8). Notice however that since downward flow occurs for a fluid pressure gradient that is less than hydrostatic, the permissible height of such a compartment is severely limited by (3.3).

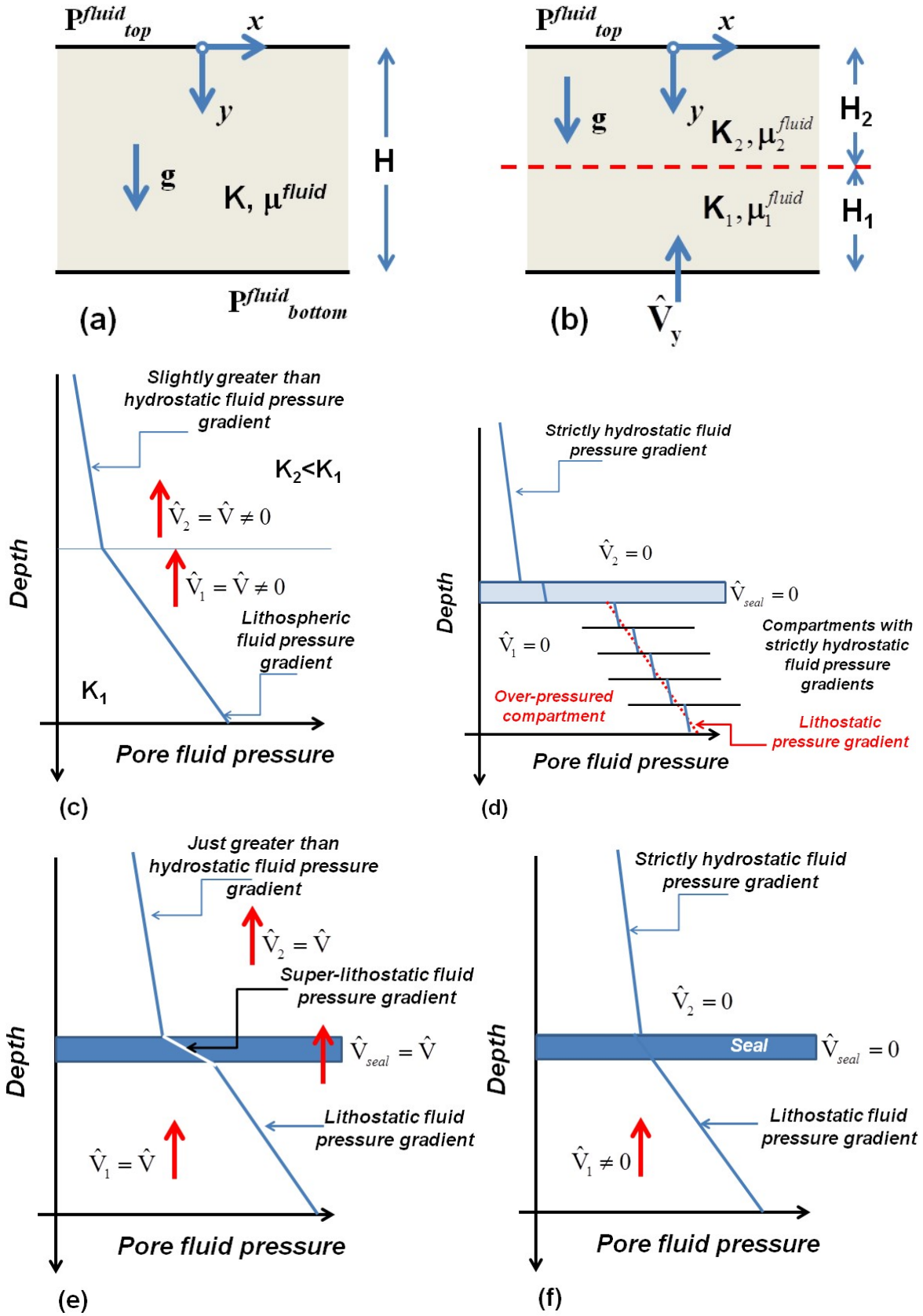

Figure 3.9. Simple models of fluid compartments in the crust. (a) A single compartment of height, H, permeability, K, and fluid viscosity, μ^{fluid}. (b) A two layer system with properties as indicated. The layers are referred to as Layer 1 (bottom) and Layer 2 (top). (c) A system with continuity of fluid flux. If $K_2 < K_1$ the fluid pressure gradient in the upper compartment can be close to hydrostatic whilst the gradient in the lower

compartment is lithostatic. A seal between the two compartments is not necessary for this transition to exist. (d) A system with zero fluid flux. Fluid pressure gradients in all compartments are hydrostatic. No upward flow. The lower compartment is over-pressured and separated from the upper compartment by a low permeability seal. This lower compartment has an average fluid pressure gradient which is lithostatic but is divided into smaller compartments where the gradient is hydrostatic. (e) Another system with continuity of fluid flux. Upper compartment with a fluid pressure gradient just above hydrostatic. Lower compartment with a lithostatic fluid pressure gradient. Fluid pressure gradient in the "seal" is super-lithostatic. Fluid flux is the same everywhere. (f) A system with no continuity of fluid flux and hence is physically unrealistic. Fluid pressure gradient in upper compartment is hydrostatic and lithostatic in lower compartment with a separating seal with no fluid flow. This model does not obey the fluid flux continuity equation, (3.16).

Now consider a crust consisting of two layers (Figure 3.9 b) in which a layer (Layer 1) with permeability, K_1, and fluid viscosity, μ_1, is overlain by another layer (Layer 2) in which the permeability is K_2 and the fluid viscosity is μ_2. We inject a fluid with upward Darcy velocity, $\hat{V}_y$, at the base of Layer 1. For continuity the fluid flux through both layers must be identical and hence we have

$$\hat{V}_y = -\frac{K_1}{\mu_1^{fluid}}\left(\frac{\partial P_1}{\partial y} - \rho_1^{fluid} g\right) = -\frac{K_2}{\mu_2^{fluid}}\left(\frac{\partial P_2}{\partial y} - \rho_2^{fluid} g\right) \qquad (3.19)$$

Thus if $\mu_1^{fluid} = \mu_2^{fluid}$ and $\rho_1^{fluid} = \rho_2^{fluid}$ then

$$\left(\frac{\partial P_2}{\partial y}\right) = \frac{K_1}{K_2}\left(\frac{\partial P_1}{\partial y}\right) + \rho^{fluid} g\left(1 - \frac{K_1}{K_2}\right) \qquad (3.20)$$

If $\left(\frac{\partial P_1}{\partial y}\right)$ is lithostatic and $\frac{K_1}{K_2} < 1$, $\left(\frac{\partial P_2}{\partial y}\right)$ is always less than hydrostatic but greater than hydrostatic. For instance, if $\frac{K_1}{K_2} = 0.1$ then

$$\left(\frac{\partial P_2}{\partial y}\right) = 0.1\left(\frac{\partial P_1}{\partial y}\right) + 0.9\rho^{fluid} g$$

If $\left(\frac{\partial P_1}{\partial y}\right)$ is lithostatic, and hence equal to 2.646 x 10^4 Pa m^{-1} then $\left(\frac{\partial P_2}{\partial y}\right)$ is 11.466 x 10^3 Pa m^{-1} which is to be compared with a hydrostatic fluid pressure gradient of 9.8 x 10^3 Pa m^{-1}. Thus the pore pressure gradient in Layer 2 is only 1.17 times the hydrostatic gradient. If the permeability in Layer 2 is 1000 times larger than in Layer 1 the fluid pressure gradient in Layer 2 is 1.0017 times hydrostatic. This is a general result. If a high permeability layer overlies a low permeability layer with an imposed fluid flux at the base of the lower layer, the low permeability layer acts as a control valve for the system so that the fluid pressure gradient in the high permeability layer is always less than in the low permeability layer and commonly close to hydrostatic. Similar arguments may be developed from (3.19) if the fluid viscosity and/or density changes between compartments.

This argument is readily extended to a multi-layered crust (Zhao et al. 1998, 2008). The overall conclusion is that it is not possible everywhere to have the fluid pressure gradient at lithostatic. The lowest permeability layer acts as a control valve for the system as a whole. Continuity of flux demands that in the highest permeability layers the fluid pressure gradient must

be below lithostatic, commonly close to hydrostatic, with no need for a low permeability "seal" between the layers.

It is important to understand the mechanical and hydrological implications of proposing a low permeability "seal" or "cap" in a system where the fluid pressure gradient is maintained below the seal at lithostatic. The lithostatic fluid pressure gradient means there must be upward flow-through in the lower layer and continuity of flux demands this same fluid flux is maintained in the seal although at a higher fluid pressure gradient (from (3.20)). This means that the fluid pressure in the cap is above lithostatic and hence the cap is prone to yielding thus reducing the fluid pressure gradient. The cap in general cannot survive in a stressed system without failure.

Four different models for a layered crust with variations in fluid pressure gradient are shown in Figures 3.9 (c) to (f). The continuity equation (3.16) permits the models in Figures 3.9 (c) to (e) but (f) is not permitted.

3.2.4. Advection of heat in porous flow.

Heat is said to be *advected* in porous flow when it is carried with the fluid. A special form of advection is *convection* when the flow is driven by density contrasts; the density contrasts may derive from thermal and/or chemical effects. When convection is driven by gradients in both temperature and density arising from chemical changes the process is known as *double diffusion driven convection* (Zhao et al., 2008, Chapter 11). When heat is advected in a steady manner the governing equations comprise [3.13], [3.14] and [3.16] together with

$$\rho_0^{fluid} c_P^{fluid} \left(\hat{V}_x \frac{\partial T}{\partial x} + \hat{V}_y \frac{\partial T}{\partial y} \right) = k_e \left(\frac{\partial^2 T}{\partial x^2} + \frac{\partial^2 T}{\partial y^2} \right) \tag{3.21}$$

where ρ_0^{fluid}, c_P^{fluid} are the reference fluid density and the fluid specific heat. The solutions to these equations are given by Zhao et al. (2008). It is convenient to introduce the following dimensionless parameters:

$$P^* = \frac{P - P_{top}}{\rho_0^{fluid} g H} \quad , \quad T^* = -\frac{\left(T - T_{top}\right) k_e}{q_0 H} \tag{3.22}$$

$$Pe^{thermal} = \frac{\rho_0^{fluid} H c_P^{fluid}}{k_e} \hat{V} \quad , \quad y^* = \frac{y}{H} = H^* \tag{3.23}$$

where $Pe^{thermal}$ is the Peclet number for the hydrothermal system. For simplicity below we write Pe for $Pe^{thermal}$. Then the solutions to the above equations become:

$$T^* = \frac{1}{Pe} \exp[Pe] \left\{ 1 - \exp\left[-Pe y^* \right] \right\} \tag{3.24}$$

and

$$P^* = y^* + \frac{q_0 \beta_T H}{k_e Pe} \exp[Pe] \left\{ y^* - \frac{1}{Pe} \left[1 - \exp\left(-Pe y^* \right) \right] \right\} - \frac{\mu \hat{V}}{K \rho_0^{fluid} g} \tag{3.25}$$

From which we obtain

$$\frac{\partial P^*}{\partial y^*} = 1 + \frac{q_0 \beta_T H}{k_e Pe} \exp[Pe] \left\{ 1 - \exp\left(-Pe y^* \right) \right\} - \frac{\mu^{fluid} \hat{V}}{K \rho_0^{fluid} g} \tag{3.26}$$

The expressions [3.24], [3.25] and [3.26] give the dimensionless temperature, pressure and fluid pressure gradients as functions of dimensionless depth. If we take the values of the various material constants and parameters given in Table 3.1 then the temperature distribution defined by (3.24) is shown in Figure 3.10 for $1 \leq Pe \leq 5$. The Figure shows that for any value of Pe above 1 the temperature at the base of the system is unacceptably high for observed temperature distributions in the crust. For Pe = 1, 2 and 5 the temperature at the base of the system is 1.7, 3.2 and 29.5 times that predicted by the conduction solution. Thus in the absence of evidence for major discontinuities in the temperature distribution with depth in the crust together with temperature values at the Moho close to what we would expect from a conduction solution, maximum values of Pe around 1 seem to be indicated. A value of $Pe \geq 1$ for the crust places severe restrictions on the physically possible values of $\hat{\mathbf{V}}$ for the crust and whether convection is possible for lithostatic pore pressure gradients; we discuss this issue in §3.7.

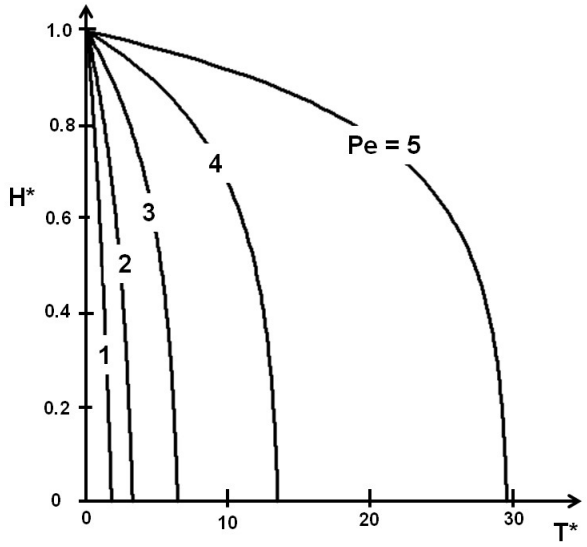

Figure 3.10. The influence of upward flow-through of fluids on the temperature distribution in a compartment with constant permeability. Plot of dimensionless height, H*, of the system against the dimensionless temperature, T*, for various Peclet numbers. For a Peclet number of 1 the temperature profile with depth is close to the conduction solution and blends into a conduction solution at the top of the compartment. For a Peclet number of 5 the temperature at the base of the system is close to 30 times what is expected of the conduction profile and there is a strong discontinuity in temperature profile with respect to a conduction gradient at the top of the compartment.

3.3. Drivers of fluid flow.

Fluid flow in porous rocks is driven by one of four processes or by combinations of these processes. The one most commonly modelled arises from hydraulic head gradients induced by *topographic gradients* (Garven and Freeze, 1984 a, b; Garven, 1985; Phillips, 1991; Murphy et al., 2008). A second process, *buoyancy* leading to convection, arises from density variations induced by temperature or chemical variations (Nield and Bejan, 2013). A third process arises from the generation of *fluid pressure gradients larger than hydrostatic* induced by compaction, devolatilisation reactions or crystallisation of volatile rich magmas (Fyfe et al., 1978; Phillips, 1991; Connolly, 2010; Burnham, 1979, 1985) and a fourth process arises from *fluid pressure gradients induced by deformation* (Ge and Garvin, 1989; Sibson,

1987, 1995; Cox, 1995, 1999; Ord and Oliver, 1997). We discuss each of these processes in turn below.

Table 3.3. Magnitudes of hydraulic head gradients driving fluid flow for various processes. The fluid is assumed to be water with a density of 1000 kg m^{-3}.

Driver	Magnitude Pa m^{-1}	Direction of flow
Lithostatic fluid pressure gradient	1.7×10^4	Vertical
5 km of topographic relief over 100 km	500	Downwards and horizontal
Deformation assuming 50 MPa gradient in fluid pressure over 1 km	5×10^4	Depends on scale of structures
Deformation assuming 50 MPa gradient in fluid pressure over 10 km	5×10^3	Depends on scale of structures

3.3.1. Topographically driven flow.

A gradient in topography for saturated porous material produces a gradient in hydraulic head which drives fluid flow in exactly the same manner as is illustrated in Figure 3.8. The system is an open flow system that is controlled by the imposed hydraulic head (Figure 1.5 d). This means that the local Darcy flow is influenced by the local permeability and fluid is focussed into the highest permeability layers, lenses or shear zones. If the local permeability changes due to clogging of pore space by mineral deposition, or to mineral dissolution or to fracturing, the local Darcy velocity changes as described by Darcy's law. In particular, if the porosity is clogged up by mineral deposition then the fluid flow stops. This form of flow is the most commonly studied in the geological literature and derives from hydrological studies in near surface aquifers (Garvan and Freeze, 1984 a, b). Except in the uppermost crust topographically driven flow is not the most important fluid driver in metasomatic systems. Such systems are commonly flow controlled open systems (see Chapter 5; Figure 5.2 c) where the flux into the system is the controlling factor rather than the hydrological head. However if large gradients in topography exist above the metasomatic system, as would arise from the presence of large mountain ranges, they would add a horizontal component to flow throughout the crust; this is true for both aqueous fluids and melts.

Examples of systems where the flow is controlled by topographic gradients are given by Garven (1985), Phillips (1991), Person and Baumgartner (1995); and Murphy et al. (2008). Lyubetskaya and Ague (2009) present examples where the flow of deep metamorphic fluids driven essentially by lithospheric pore pressure gradients is influenced by large topographic gradients.

3.3.2. Systems with super-hydrostatic fluid pressure gradients. Production of fluid and the pressure control valve.

The argument presented below is developed for partial melt systems by Hobbs and Ord (2012, 2015). We do not repeat the argument here but only present the results for fluids that are not melts. Following Phillips (1991) we consider mineral reactions of the form:

$$S_1 \rightarrow S_2 + fluid$$

where the fluid may be a hydrous fluid, CO_2 or some other fluid. S_1 is an assemblage bearing an initial volume concentration, s_o, of a hydrous phase such as muscovite, biotite or amphibole and S_2 is an anhydrous assemblage. In this reaction, s cubic meters of a cubic meter of the assemblage S_1 decrease with time as they are replaced by S_2.

The total rate of generation of fluid in this reaction zone (volume of fluid per unit time per unit area of the reacting zone) is

$$\Re^{fluid} = \int_0^\infty Q^{fluid} d\xi = n^{fluid} \mathrm{U} s_o$$

where Q^{fluid} is the volumetric rate of fluid generation at the devolatilising front, U is the rate at which the reaction isotherm rises in the crust and s_o is the initial volumetric concentration of the phase that devolatilises. $\Re^{fluid}$ is independent of the reaction rate, γ, and of the temperature gradient, *grad*T.

If the porosity of the rock is constant, the vertical flux of fluid, $\hat{\mathrm{V}}$, at the top of the reaction zone is the volume of fluid produced per unit time per unit horizontal area or $\Re^{fluid}$. Thus if y is the vertical distance above the reaction isotherm, the vertical gradient of the total fluid pressure at the top of the reaction zone is

$$\frac{\partial \mathrm{P}^{fluid}}{\partial y} = -\frac{\mu^{fluid}}{\mathrm{K}} \hat{\mathrm{V}} - \rho^{fluid} \mathrm{g} = -\frac{\mu^{fluid}}{\mathrm{K}} \Re^{fluid} - \rho^{fluid} \mathrm{g}$$

where P^{fluid} is the total fluid pressure, μ^{fluid} is the fluid viscosity, K is the vertical permeability, ρ^{fluid} is the density of the fluid and g is the acceleration due to gravity. This pressure is a constant once the isotherm has risen a distance equal to the thickness of the reaction zone and the fluid pressure induced by the upward flow diffuses upwards according to:

$$\frac{\partial \hat{\mathrm{P}}^{fluid}}{\partial t} = \kappa^{fluid} \frac{\partial^2 \hat{\mathrm{P}}^{fluid}}{\partial y^2} \qquad (3.27)$$

where κ^{fluid} is the pressure diffusivity of the fluid and $\hat{\mathrm{P}}^{fluid}$ is the *reduced pressure* defined as $\hat{\mathrm{P}}^{fluid} = \mathrm{P}^{fluid} + \rho_0^{fluid} \mathrm{g} y$ where ρ_0 is the average density of the fluid and y is directed vertically upwards. $\hat{\mathrm{P}}^{fluid}$ is always greater than the hydrostatic fluid pressure and with increase in time becomes super-lithostatic (Phillips, 1991) if the initial permeability of the rocks above the devolatilisation zone is small enough and/or μ^{fluid} $\Re^{fluid}$ is large enough. It is easy to see however that if any or a combination of any of the following occur, then the fluid pressure at the reaction front evolves to a new value: (i) the fluid producing reaction alters, (ii) the upward velocity, U, of the reaction isotherm changes, (iii) the modal concentration of the hydrous phase changes thus altering s_o. Thus the processes occurring near the devolatilisation front control the pressure at the reaction front and hence the pressure distribution throughout the devolatilisation system. Notice also from this argument that it is the upward velocity of the fluid, $\hat{\mathrm{V}}$, that is controlled by these processes. The permeability is a dependent variable that has to evolve, by compaction or positive dilation, to a value that accommodates this flux given the fluid pressure gradient that develops.

The solution to (3.27) is given in Figure 3.11 where the dimensionless height, y/H, is plotted against the dimensionless value of the reduced pressure, expressed as $\frac{\hat{P}^{fluid}K}{\mu^{fluid}\Re^{fluid}H}$, for a system where a low permeability compartment is overlain by a higher permeability layer. The lithospheric minus the hydrostatic gradient is indicated by the solid red line which has a slope of $\tan^{-1}(1/1.7)$, the gradient of the reduced pressure being 1.7 x 10^4 Pa m^{-1}. The contours of dimensionless fluid pressure are given in terms of the dimensionless time (tH^2/κ^{fluid}). The positions for each time where the reduced pressure gradient passes upward from super-lithostatic to sub-lithostatic are shown as open dots and the evolution of the super-lithostatic front with time is shown by the red arrow. By dimensionless time 0.6 the whole compartment is lithostatically pressured and from then on the compartment is pressured above lithostatic.

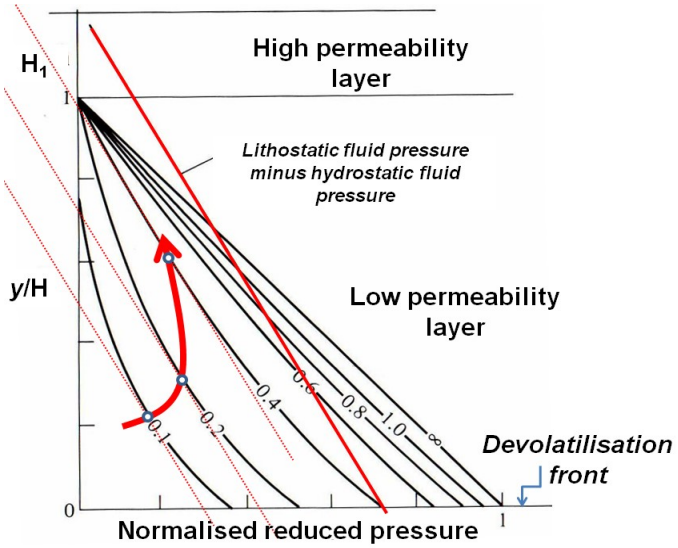

Figure 3.11. Diffusion of fluid pressure from a devolatilisation front. (After Phillips, 1991). Plot of non-dimensional depth against non-dimensional reduced fluid pressure at dimensionless times (tH^2/κ^{fluid}). The red arrow shows the progressive rise of the lithostatically pressured fluid front above the devolatilisation front.

3.3.3. Deformation driven flow.

Fluid flow driven by deformation arises from two processes that influence the local pore pressure. This can be seen from the following argument. Formally, the fluid mass balance is:

$$\frac{\partial \zeta}{\partial t} = -\frac{\partial \hat{V}_i}{\partial x_i} + q_V \qquad (3.28)$$

where $\hat{V}_i$ are the components of the Darcy flux, q_V is the flux of fluid per unit volume of the porous material and ζ is the *variation of fluid content* (see Detournay and Cheng, 1993; Coussy, 1995) which can be thought of as the "hydraulic strain" associated with the introduction of fluid; ζ is defined as the variation of fluid volume per unit volume of porous material and hence is dimensionless. A positive ζ means a gain in fluid content by the porous material.

As well as (3.28) which expresses the mass balance of fluid we need a relation for the balance of momentum that is a function of the local porosity, ϕ:

$$\frac{\partial \sigma_{ij}}{\partial x_j} + \rho g_i = \rho \frac{\partial \dot{u}_i}{\partial t} \tag{3.29}$$

where $\rho = (1-\phi)\rho^{solid} + \phi\rho^{fluid}$ and ρ^{solid}, ρ^{fluid} are the densities of the solid and fluid phases respectively.

The change in the fluid pressure, P^{fluid}, is then given by:

$$\frac{\partial P^{fluid}}{\partial t} = M\left(\frac{\partial \zeta}{\partial t} - \alpha \frac{\partial \varepsilon_V}{\partial t}\right) \tag{3.30}$$

where ε_V is the volumetric strain that can arise from both deformation and chemical reactions: $\varepsilon_V = \varepsilon_V^{deformation} + \varepsilon_V^{chemical\ reactions}$. M and α (Detournay and Cheng, 1993) are material parameters known as the *Biot modulus* and the *Biot coefficient* respectively. If the compressibility of the solid grains can be neglected compared to that of the fluid then we can take $\alpha = 1$ and

$$M = \frac{K^{fluid}}{\phi} \tag{3.31}$$

where K^{fluid} is the bulk modulus of the fluid. Thus the change in fluid pressure is given by

$$\frac{\partial P^{fluid}}{\partial t} = \frac{K^{fluid}}{\phi}\left(\frac{\partial \zeta}{\partial t} - \frac{\partial \varepsilon_V}{\partial t}\right) \tag{3.32}$$

Expressions (3.28), (3.29) and (3.32) are sufficient to describe the influence of deformation and chemical reactions on fluid flow. Note that the mean stress on the solid does not enter into these equations. It is sometimes claimed (for example, Ridley, 1993) that fluid flow is driven by mean stress gradients the implication being that the fluid pressure is locally equal to the mean stress. This however is not generally true; fluid flow is driven by gradients in fluid pressure (in the absence of gravity) and so is strongly influenced by local changes in porosity which arise from changes in stress (Detournay and Cheng, 1993) and from changes in pore volume as expressed by (3.32).

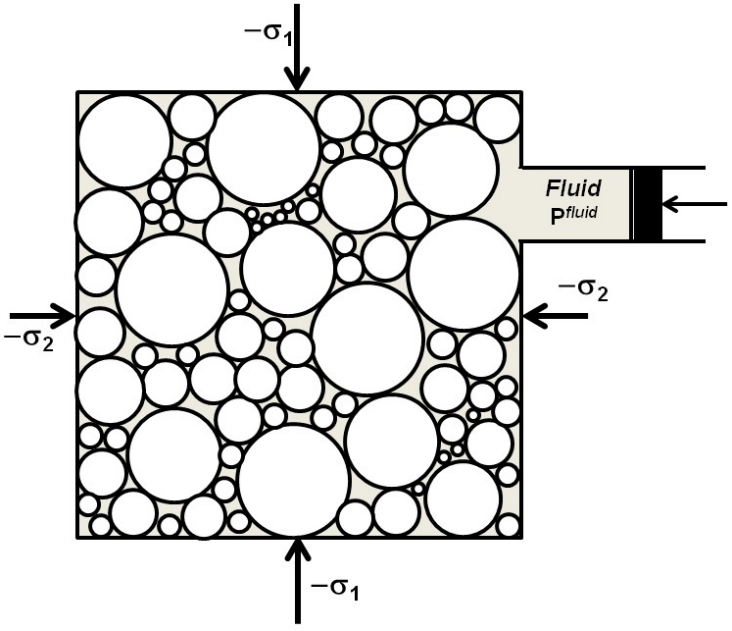

Figure 3.12. A 2D closed system consisting of an aggregate of disc shaped grains immersed in a fluid. The pore pressure, P^{fluid}, is controlled by a moveable piston. An externally imposed stress is σ_{ij}. We imagine the stresses in the grains are elastic stresses. The mean stress in this case is $\overline{P} = -(\sigma_{11} + \sigma_{22})/2$. Clearly the fluid pore pressure can be set to any value independently of the mean stress. The only restrictions on the fluid pressure is that it should not exceed the smallest principle stress when failure of the aggregate results. For low fluid pressures the stresses at grain contacts should not be such as to cause plastic flow.

In cases where the system is closed (undrained) or open (drained) and elastic then $\varepsilon_V = \frac{\overline{P}}{K}$ and the mean stress, $\overline{P} = -(\sigma_{11} + \sigma_{22} + \sigma_{33})/3$, is related to the elastic volumetric strain, ε_V, by

$$\varepsilon_V = \frac{\overline{P}}{K}$$

where K is the undrained or drained bulk modulus of the solid.

This means that for the closed system case, where $\frac{\partial \zeta}{\partial t} = 0$, changes in mean stress are linearly related to changes in pore pressure and to say that fluid flow is driven by gradients in pore pressure is equivalent to saying that fluid flow is driven by gradients in mean stress. However, we emphasise, that this is true only for closed elastic materials. An example of such a situation is given in Figure 3.13 (a, b, c). In the open case $\frac{\partial \zeta}{\partial t} \neq 0$ and in general the pore pressure is no longer linearly related to the mean stress (Figures 3.13 d, e, f).

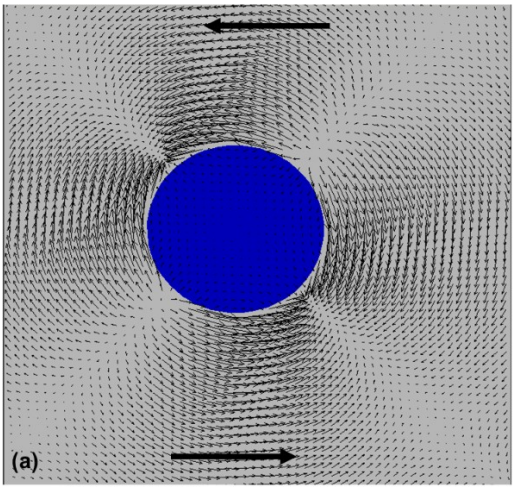

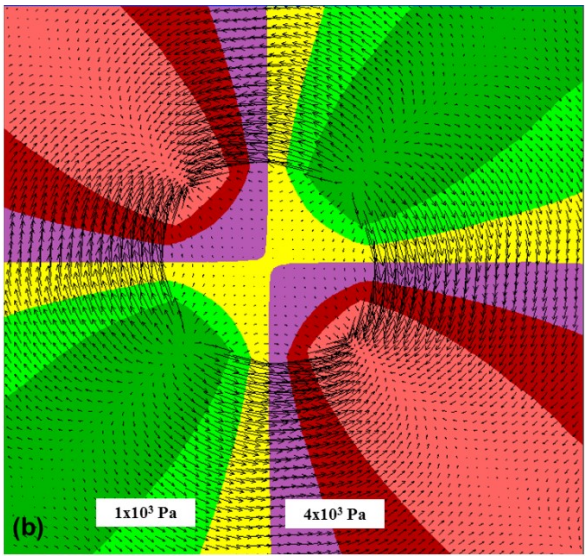

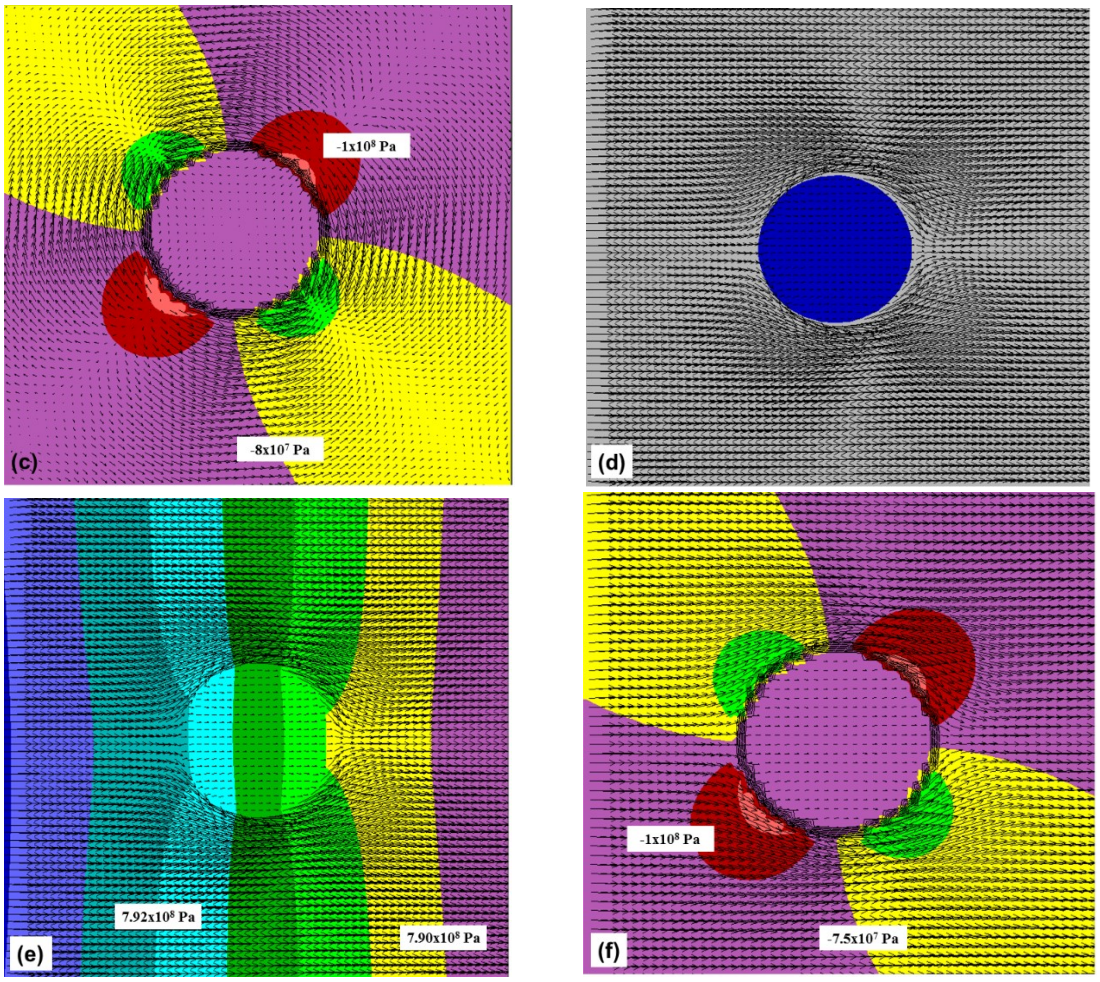

Figure 3.13. Control of fluid flow in elastic systems. (a), (b) and (c) is a closed fluid saturated material undergoing sinistral shearing as indicated by the arrows in (a); (d), (e) and (f) is an open system with fluid flow from left to right and undergoing the same sinistral shearing as in (a). A circular inclusion with bulk and shear moduli 10^{12} Pa is embedded in an elastic matrix with bulk and shear moduli 10^{11} Pa. The permeability of the matrix is 10^{-18} m^2 and that of the disc is 10^{-19} m^2. Contour intervals in the various diagrams are (b): $1.0x10^3$ Pa , (c): $2.0x10^7$ Pa (e): $5.5x10^5$ Pa, (f): $2.5x10^7$ Pa.

In Figure 3.13 (a, b, c) fluid flow is from regions of high pore pressure to regions of low pore pressure. Since the system is closed and the deformation is elastic this corresponds to flow from regions of high mean stress to regions of low mean stress. Notice that the patterns of fluid pressure in (b) differs from the pattern of mean stress in (c). The maximum Darcy flow vector in is $5.5x10^{-13}$ ms^{-1}. In the elastic open system (Figures 1.3 d, e, f) fluid flow is strictly down the gradient in pore pressure as shown in (e) and crosses the contours of mean stress obliquely as in (f). The maximum Darcy flow vector is 4.2 $x10^{-11}$ ms^{-1}. The relatively small magnitude of Darcy flow in closed systems relative to open systems with geologically realistic pore pressure gradients is the common situation (Ge and Garven, 1992).

Figure 3.14 is presented as an example to demonstrate the effects of local plastic dilation on the distribution of pore pressure. In this example a material with Mohr-Coulomb dilatant constitutive properties undergoes sinistral simple shearing with an imposed fluid pressure gradient from left to right. The fluid focuses into regions of positive volumetric strain rate and shows no relation to the mean stress. These effects have been shown to be

important at a regional scale by Ord and Oliver (1997). In general the fluid pressure cannot reach the mean stress in value without yield occurring as shown in Figure 3.3 (b and d).

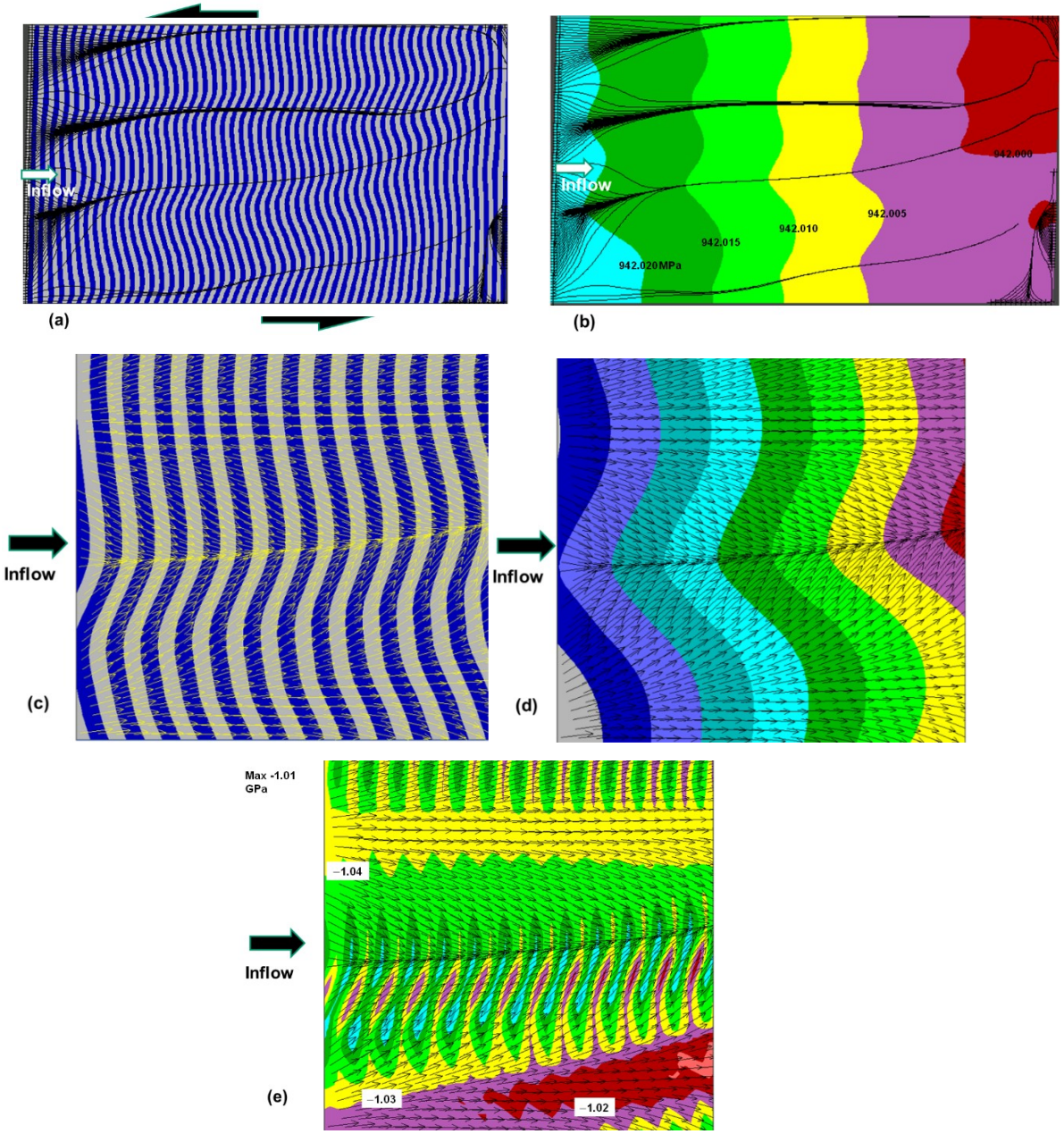

Figure 3.14. Control of fluid flow by pore pressure perturbations related to volumetric strains. Multi-layer model deformed by simple shearing with pore pressure gradient from left to right. Mohr-Coulomb material with dilation. Layers are defined by two different values of cohesion. (a) Stream lines superimposed on geometry of deformation. (b) Stream lines superimposed on contours of pore pressure. (c) Central section from the model. Plots of flow vectors (yellow) superimposed on geometry. Flow is concentrated along the axial plane of a weak fold. (d) Plots of flow vectors superimposed on contours of fluid pore pressure. Same section of model as (c). The flow is down the pore pressure gradient at all places. (e) Plots of flow vectors superimposed on contours of mean stress. Same section of model as (c). There is no correlation between flow and mean stress. Material properties are: Cohesion: 10 MPa. Friction angle: 30°. Dilation angle: 10°. Pore pressure gradient: 1.08×10^{4} Pa m^{-1} from left to right. Shearing strain-rate: 1.08×10^{-8} s^{-1}.

In summary, fluid flow is driven by gradients in mean stress *only* in closed elastically deforming systems. This is because in this specific case the fluid pressure is a linear function

of the mean stress and the only contribution to volume change is the elastic volume change. In open elastic systems (in the absence of gravity) fluid flow is driven by gradients in fluid pore pressure and is independent of gradients in mean stress. In open elastic-plastic systems again fluid flow is driven by gradients in fluid pressure which may locally be strongly influenced by volume changes arising from plastic dilation Again, the fluid flow is independent of gradients in mean stress.

The common example of the influence of deformation upon fluid flow that we explore in a little detail is the *fault-valve* and *seismic pumping* models proposed by Sibson (1981,1987, 2001, 2004) and extended by Cox (1995, 1999) and Cox et al. (2001). These models involve a fault that crosses a seal between one compartment (above) and another (below) which is over-pressured below the seal; the fault acts as a valve in which the permeability decreases during fault slip. Notice, although not commonly appreciated, that these models can only apply to the situation pictured in Figure 3.12(d) and not Figures 3.12 (c, e, f). The models propose a seismic event that decreases the permeability in the fault so that fluid is driven upwards from the over-pressured compartment beneath. The fault then seals but can reactivate in subsequent seismic events thus resulting in seismic pumping from one compartment to the other. A number of workers (Matthai and Fischer, 1997; Matthai and Roberts, 1991, Braun et al., 2003; Sheldon and Ord, 2005; Weatherley and Henley, 2013) have explored the mechanics of these models with particular emphasis on the dilation associated with the faulting event. Sheldon and Ord (2005) model the fault valve process and show that if the fault zone is dilatant, fluid may be sucked into the fault zone rather than be simply transferred from the over-pressured compartment to the overlying compartment. Weatherley and Henley (2013) couple this process strongly to the magnitude of the seismic event associated with faulting and show that the increase in volume associated with such events can lead to boiling and subsequent deposition of minerals such as quartz and gold as a result of the phase change.

3.4. Focussing of fluid flow.

When a lens of relatively high permeability, in the form of a sedimentary lens, a fault zone or an individual fracture, is embedded in a material of lower permeability, the fluid flow is focussed into the lens as shown in Figure 3.15 (a). The reason for this is that, neglecting the effect of gravity, the Darcy flow is higher in the lens than in the embedding material for the same pore pressure gradient. This initiates a pore pressure gradient around the lens that enhances the focussing effect. The mathematical formulation is identical to that in many heat flow problems. Again, neglecting the effect of gravity, the governing equations in two dimensions are the continuity equation and the two equations describing Darcy flow:

$$\frac{\partial \hat{\mathrm{V}}_x}{\partial x} + \frac{\partial \hat{\mathrm{V}}_y}{\partial y} = 0 \qquad (3.33)$$

$$\hat{\mathrm{V}}_x = \frac{\mathrm{K}}{\mu^{fluid}}\left(-\frac{\partial \mathrm{P}^{fluid}}{\partial x}\right) \qquad (3.34)$$

$$\hat{\mathrm{V}}_y = \frac{\mathrm{K}}{\mu^{fluid}}\left(-\frac{\partial \mathrm{P}^{fluid}}{\partial y}\right) \qquad (3.35)$$

Substitution of (3.34) and (3.35) into (3.33) gives:

$$\frac{\partial^2 \mathrm{P}^{fluid}}{\partial x^2} + \frac{\partial^2 \mathrm{P}^{fluid}}{\partial y^2} = 0 \qquad (3.36)$$

which is the classical Laplace's equation, commonly used in heat flow problems (Carslaw and Jaeger, 1959) and in many branches of physics (Boyce and DiPrima, 2005, pp 638-655). Solutions to this equation for complicated geometries usually require numerical methods. The analytical solution for a sphere is discussed by Phillips (1991, pp 68-69) and Zhao et al. (2008, Chapters 6, 7 and 8) present analytical solutions for an elliptical lens of low permeability embedded in a higher permeability material of any orientation with respect to the imposed flow direction and with thermal transport. Some results of modelling fluid focussing are presented in Figures 3.15.

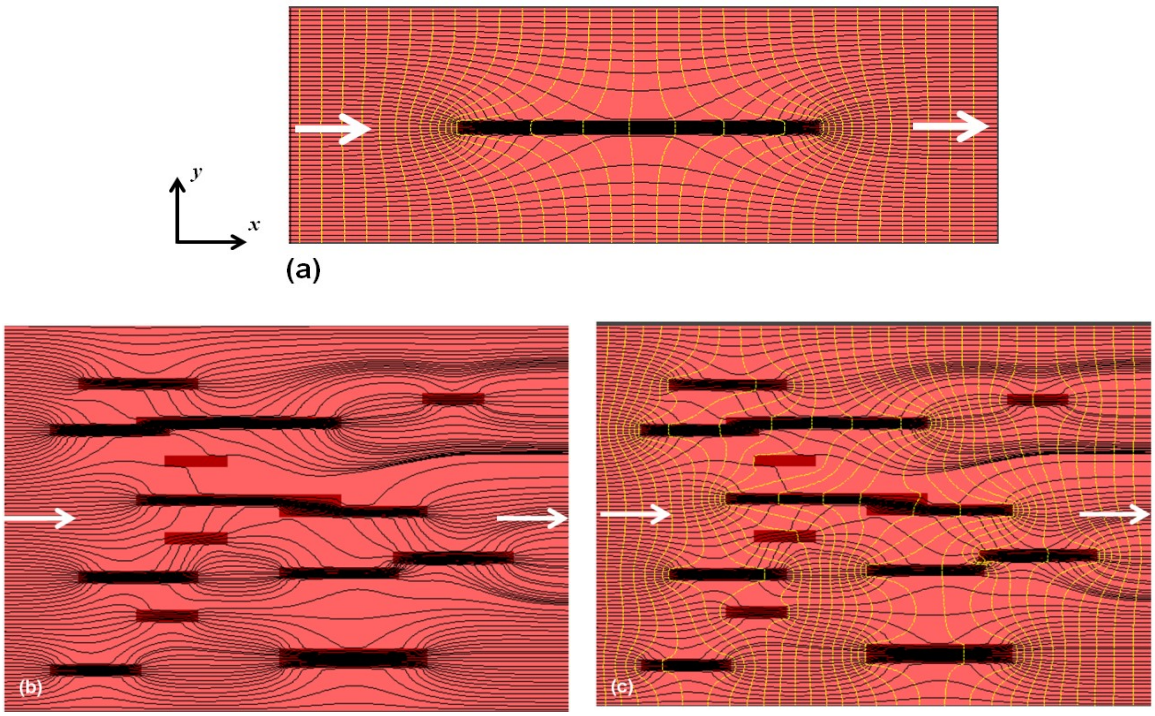

Figure 3.15. Focussing of fluid flow into lenses. Streamlines in black, pore fluid pressure contours in yellow. White arrows show the direction of flow. (a) A single lens. (b), (c) Multiple lenses. Fluid pressure contours added in (c). The permeability in the lenses is an order of magnitude higher than in the matrix.

An important measure of such fluid focussing is the degree of fluid focussing measured by the parameter Λ. This is given for an elliptical lens with major axis a and minor axis b and aspect ratio $\mathrm{A} = \frac{a}{b}$ and permeability ratio $\Pi = \frac{\mathrm{K}^{lens}}{\mathrm{K}^{matrix}}$ by

$$\Lambda = \frac{\mathrm{A}(\Pi + 1)}{\Pi + \mathrm{A}} \qquad (3.37)$$

where K^{lens} and K^{matrix} are the permeabilities inside the lens and for the matrix.

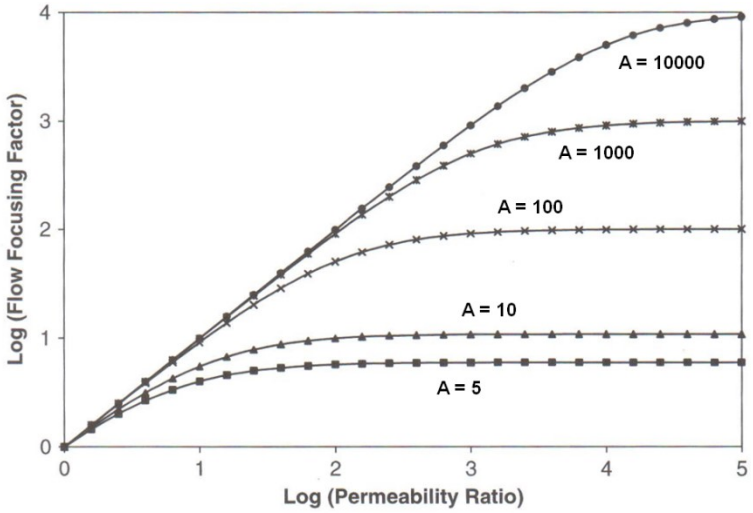

Figure 3.16. Focussing factor for an elliptical lens with long axis parallel to the direction of flow. After Zhao et al. (2008). A is the aspect ratio of the high permeability elliptical lens.

Figure 3.16 shows the degree of fluid focussing for a lens oriented with its long axis parallel to the flow. One can see that a lens with aspect ratio of 100 (a thin crack) results in fluid focussing close to 180 for a permeability ratio of 100. Other examples are given by Zhao (2008). These effects have been emphasised by Lyubetskaya and Ague (2009) and Ague (2011) in discussions of high fluid fluxes in metamorphic rocks.

3.5. Convective flow.

If fluid density variations exist within a porous medium in a gravity field then it is possible that flow instabilities arise in order to homogenise the density fluctuations. Such density variations can arise from chemical or thermal fluctuations. Here we consider only density variations arising from thermal effects. The unstable flow that arises in such systems is called *convection.* The nature of the convective flows that form depends both on the geometry of the system and its boundary conditions. If we consider a system, such as that shown in Figure 3.17, where the sides of the system stretch to infinity, then boundary conditions at the top and bottom of the system can consist of various combinations of fixed temperature and fluid pressure or fixed heat flow and fluid flow (Nield and Bejan, 2013). We consider two of these combinations below. In the first instance (Figure 3.17 a) temperature and fluid pressure are fixed at the top and bottom of the system such that $T_{top} < T_{bottom}$ and the initial fluid pressure gradient is hydrostatic. This corresponds to the classical Horton-Rodgers-Lapwood model (Horton and Rodgers, 1945; Lapwood, 1948) and is the type of system envisaged by Etheridge et al. (1983). In the second instance (Figure 3.17 b) fluid and heat fluxes are fixed at the bottom of the system and temperature and fluid pressure are fixed at the top. We refer to such a system as one characterised by *upward flow-through* and consider such systems in detail in §3.5.3. Such upward flow-through systems must be the situation for compartments with lithospheric fluid pressure gradients.

We define the variation in fluid density with temperature by what is called the *Oberbeck-Boussinesq approximation*:

$$\rho^{fluid} = \rho_0^{fluid}\left[1-\beta_T^{fluid}\left(T-T_0\right)\right] \qquad (3.38)$$

where ρ_0^{fluid} is the fluid pressure at temperature T_0 and β_T^{fluid} is the thermal volume expansion coefficient of the fluid. The system is stable, that is, heat transfer takes place solely by conduction through the saturated solid, if the Rayleigh number, Ra_T, defined in (3.7) is less than a critical value which is labelled $Ra_T^{critical}$. If $Ra_T > Ra_T^{critical}$ then convective instabilities arise as shown in Figure 3.18. In (3.11) we point out that for the values of various parameters given in Table 3.1 for water Ra_T = 2.66 x 10^9 $(\Delta T)KH$ so that the Rayleigh number is proportional to the temperature difference between the top and bottom of the system, the permeability of the porous medium and the height of the system.

The critical Rayleigh number for the two dimensional system illustrated in Figure 3.18 (a) is $4\pi^2$ or 39.48 (Nield and Bejan, 2013, Chapter 6) so that, using (3.11) and the values in Table 3.1 for water a system 1 km high with a permeability of 10^{-13} m^2 becomes unstable when $\Delta T = T_{bottom} - T_{top}$ = 148.4 C^o. We consider convection is systems with upward flow through in § 3.5.3.

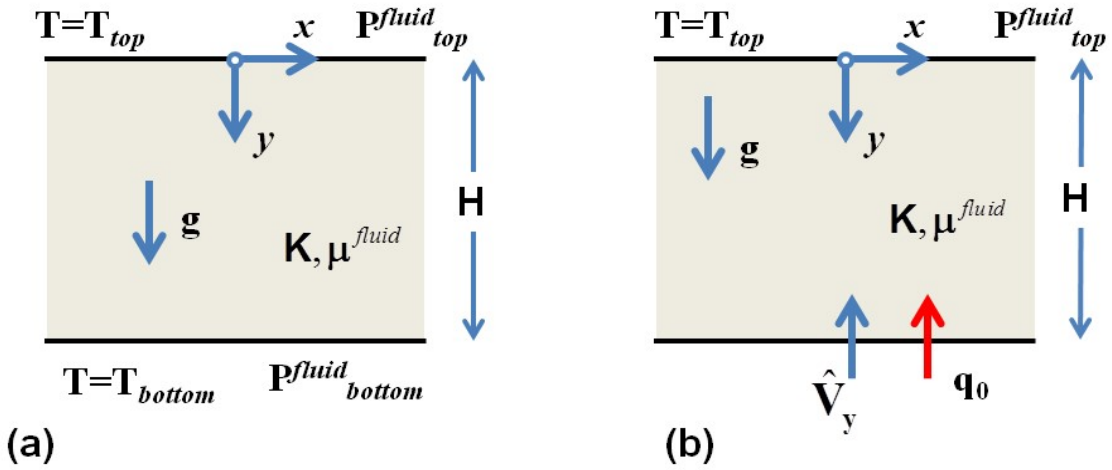

Figure 3.17. Models for thermal convection with two different boundary conditions. (a) A closed system with temperature and fluid pressure fixed at top and bottom of the system. (b) An open system where a fluid flux, $\hat{V}$, and heat flux, q_0, are applied to the base of the system and the temperature and fluid pressure are fixed at the top of the system.

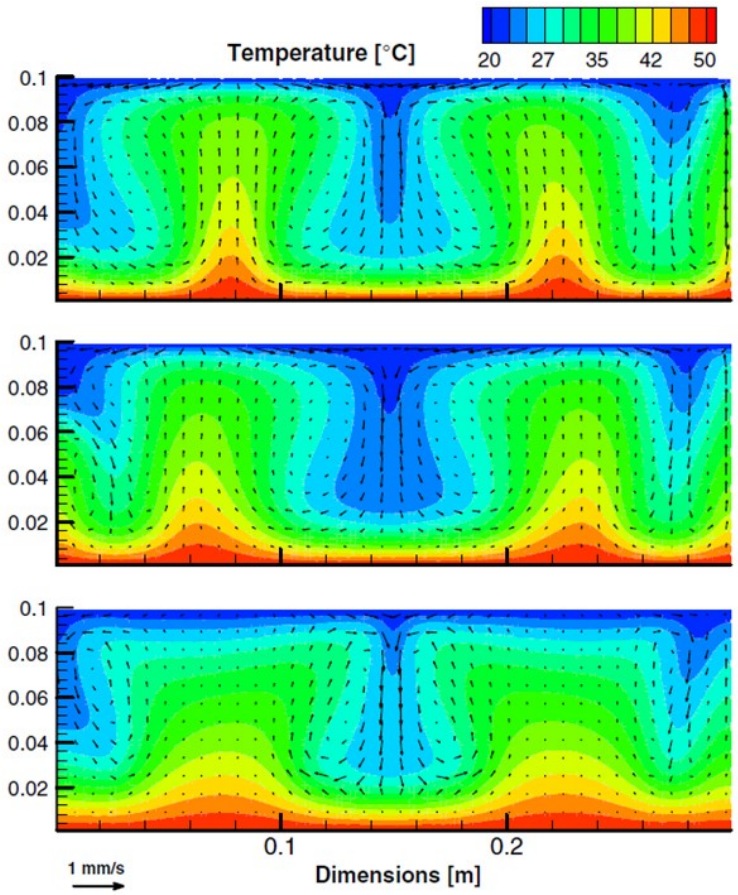

Figure 3.18. Two dimensional thermal convection showing temperature and fluid flow field evolution resulting from dissolution and precipitation of anhydrite. From Kuhn (2009). See that book for details.

3.5.1. Three dimensional convective flow.

Thermal convection in three dimensional systems with temperature and fluid pressure fixed at the top and bottom of the system is treated by Zhao et al. (2009; Chapter 2). Again, the system becomes unstable at a critical Rayleigh number which is a function of the system geometry and boundary conditions. In general the flow pattern consists of a three dimensional array of upward and downward flow domains whose geometry depends on the value of the Rayleigh number. Figure 3.19 shows results for a three dimensional system 3km high and 50 km in length with homogeneous permeability, an initial hydrostatic fluid pressure gradient and different salinities. For details of the simulations see Sheldon et al. (2010).

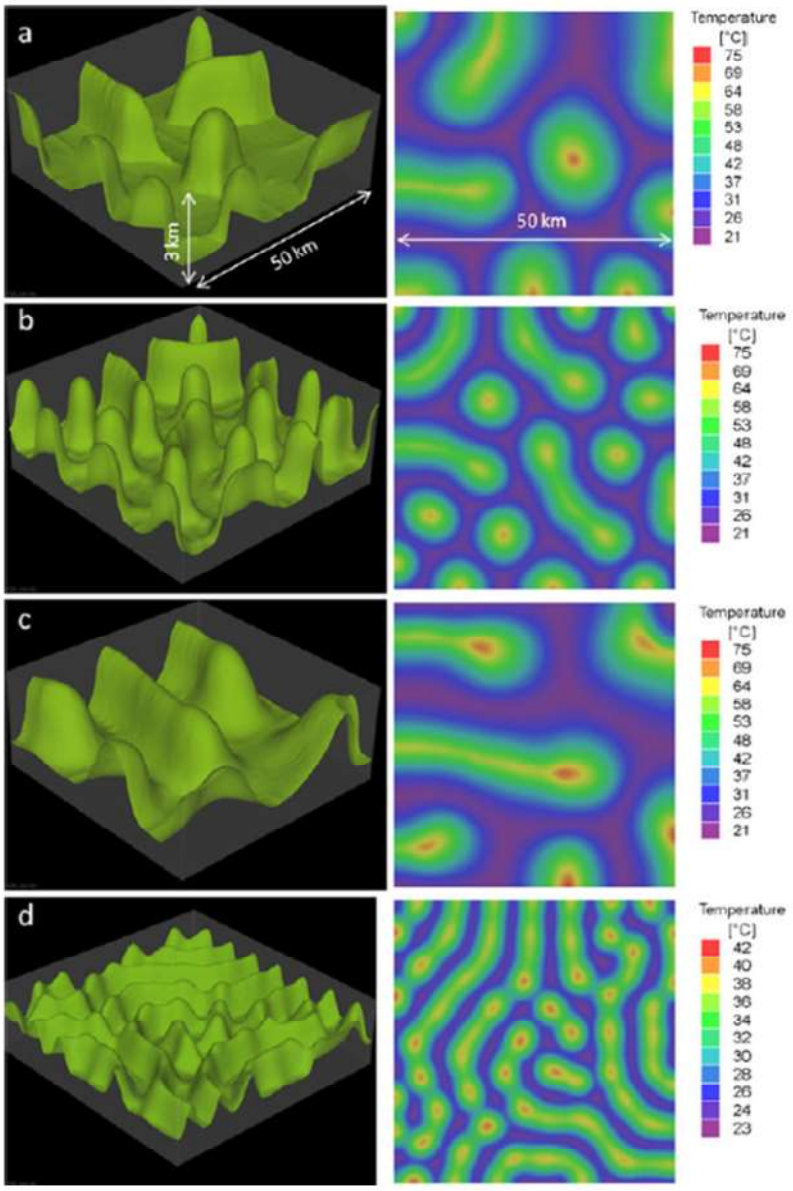

Figure 3.19. Fluid convection in a three dimensional system. Three dimensional view of convective system with temperature scale indicated on the right. System is 3 km high. Temperature isosurfaces of 60°C in (a to c); 40°C in (d). Vertical exaggeration, 5. The right hand column shows horizontal sections through the system at 567 m depth in (a to c) and 460 m in (d). From Sheldon et al. (2012). See that paper for further details.

3.5.2. Convective flow in faults.

Many metasomatic systems provide evidence that faults or shear zones have been sites for focussed fluid flow including both aqueous fluids (Beach and Fyfe, 1972; Blenkinsop and Kadzviti, 2006) and melts (Brown and Solar, 1998). The question arises: *What are the conditions for thermal convection and what are the fluid flow distributions resulting from convection in faults and shear zones*? The situation for fault zones heated from below has been extensively investigated by Zhao et al. (2008, Chapters 8 to 11). A model for the geometry of a vertical fault zone is shown in Figure 3.20, the important geometrical parameters being the length, H_1, the width, H_2, and the height, H_3, of the fault zone. For the coordinate system shown in Figure 3.20, with gravity acting parallel to the *z*-axis, the governing equations are:

$$\frac{\partial \hat{V}_x}{\partial x}+\frac{\partial \hat{V}_y}{\partial y}+\frac{\partial \hat{V}_z}{\partial z}=0 \tag{3.39}$$

$$\hat{V}_x=\frac{K_x}{\mu^{fluid}}\left(-\frac{\partial P^{fluid}}{\partial x}\right),\ \hat{V}_y=\frac{K_y}{\mu^{fluid}}\left(-\frac{\partial P^{fluid}}{\partial y}\right),\ \hat{V}_z=\frac{K_z}{\mu^{fluid}}\left(-\frac{\partial P^{fluid}}{\partial z}+\rho^{fluid}g\right) \tag{3.40}$$

$$\rho_0^{fluid}c_P\left(\hat{V}_x\frac{\partial T}{\partial x}+\hat{V}_x\frac{\partial T}{\partial y}+\hat{V}_x\frac{\partial T}{\partial z}\right)=\left(k_{ex}\frac{\partial^2 T}{\partial x^2}+k_{ey}\frac{\partial^2 T}{\partial y^2}+k_{ez}\frac{\partial^2 T}{\partial z^2}\right) \tag{3.41}$$

$$\rho^{fluid}=\rho_0^{fluid}\left[1-\beta_T^{fluid}\left(T-T_0\right)\right] \tag{3.42}$$

$$k_{ex}=\phi k^{fluid}+\left(1-\phi\right)k_x^{solid},\ k_{ey}=\phi k^{fluid}+\left(1-\phi\right)k_y^{solid},\ k_{ez}=\phi k^{fluid}+\left(1-\phi\right)k_z^{solid} \tag{3.43}$$

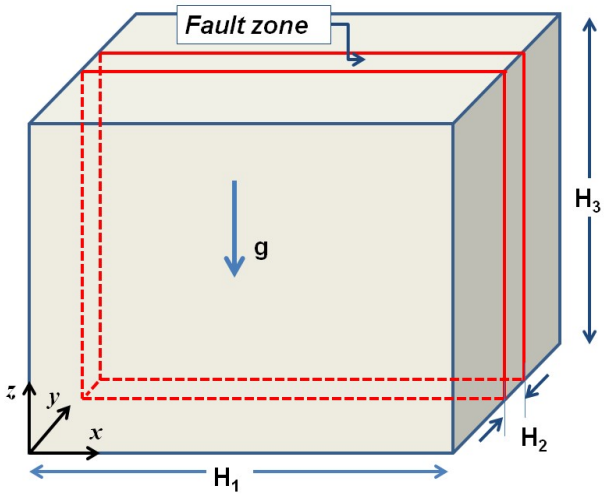

Figure 3.20. Geometry of the fault zone problem.

These equations are solved (Zhao et al., 2008, pp 146-156) for an isotropic, homogeneous porous medium with no upward flowthrough and temperatures fixed at top and bottom. The Rayleigh number for the fault is as given in (3.7) but now it is possible that convective instabilities can form in all of the *x*-, *y*- and *z*-directions. Dimensionless wave numbers are defined for these three directions as:

$$k_1^*=\frac{m\pi}{H_1^*},\ k_2^*=\frac{n\pi}{H_2^*},\ k_3^*=q\pi \tag{3.44}$$

with $$H_1^*=\frac{H_1}{H_3} \quad \text{and} \quad H_2^*=\frac{H_2}{H_3}. \tag{3.45}$$

and *m*, *n*, *q* take the values 1, 2, 3,…..

A number of different convective instabilities are possible in the fault zone. The critical Rayleigh numbers for the system are given by

$$\mathrm{Ra}_{\mathrm{T}}^{critical} = \frac{\left[\left(\frac{m\mathrm{H}_3}{\mathrm{H}_1}\right)^2 + \left(\frac{n\mathrm{H}_3}{\mathrm{H}_2}\right)^2 + q^2\right]^2 \pi^2}{\left(\frac{m\mathrm{H}_3}{\mathrm{H}_1}\right)^2 + \left(\frac{n\mathrm{H}_3}{\mathrm{H}_2}\right)^2} \qquad (3.46)$$

The smallest critical Rayleigh number is found by setting $m = n = q = 1$ and allowing H_1 to vary. It is found that the minimum critical Rayleigh number occurs as $\mathrm{H}_1 \rightarrow \infty$ when (3.44) gives a zero wave number in the x-direction.

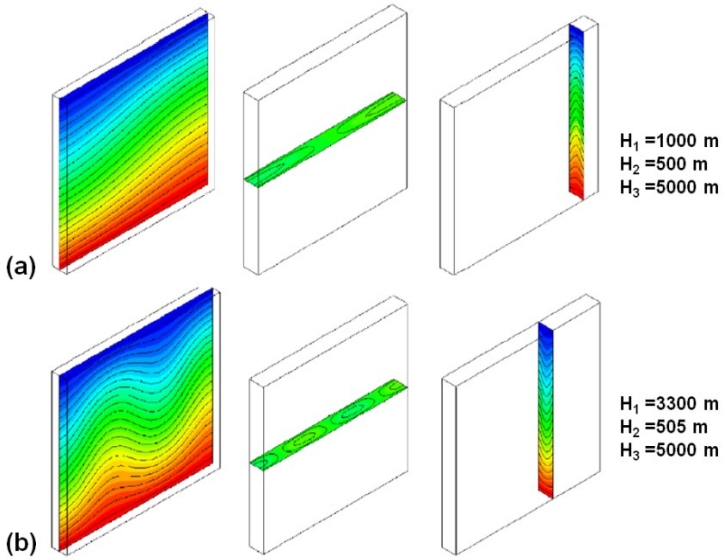

Figure 3.21. Sketches of temperature distribution patterns associated with convective flow patterns in vertical fault zones. (a) Fundamental mode. (b) Finger-like mode. After Zhao et al. (2004).

Although a number of critical Rayleigh numbers can be defined for the problem shown in Figure 3.21 some calculations using the numbers in Table 3.1 for water (Zhao et al., 2008, §9.3) show that these Rayleigh numbers are quite close to each other in magnitude so that the linear stability analysis that produces (3.46) does not necessarily indicate which instability (Figure 3.21) will grow to finite size. Modelling shows that in many instances the 3D-finger type instability is the mode that grows with critical Rayleigh numbers given by

$$\mathrm{Ra}_{\mathrm{T}}^{critical-3D-finger} = \frac{\left[m^2 + \left(\frac{\mathrm{H}_3}{\mathrm{H}_2}\right)^2 + 1\right]^2 \pi^2}{m^2 + \left(\frac{\mathrm{H}_3}{\mathrm{H}_2}\right)^2} \qquad (3.47)$$

An example is shown in Figure 3.22. Figure 3.22 (d, e) show the temperature and flow regime for the rocks surrounding the fault and the distribution of SiO_2 deposition that is associated with the temperature and flow regime.

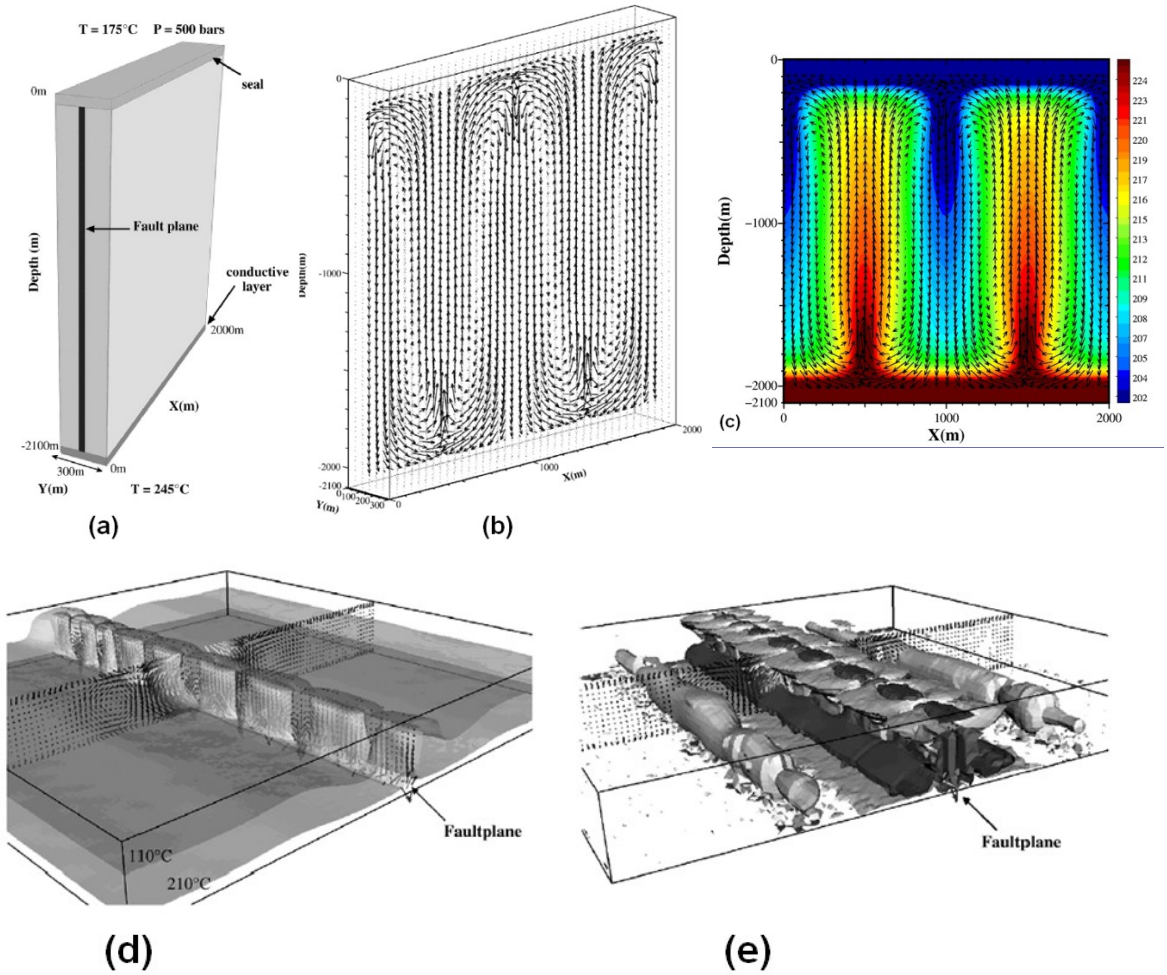

Figure 3.22. Convection and mineral reactions in three dimensional faults. (a) Geometry of the situation. (b) Darcy flow vectors. (c) Temperature distribution. (d) A three dimensional fault showing Darcy flow vectors and temperature distribution. Two temperature iso-surfaces are shown: for 110°C and 210°C. (e) Pattern of quartz deposition for the geometry shown in (d). From Alt-Epping and Zhao. (2010). See that paper for details.

If the fault is not vertical (Figure 3.23 a) and dips at an angle, φ, then the critical Rayleigh number depends on the geometry of the fault as shown in Figure 3.23 (b). Decreasing the dip angle stabilises the flow so that $Ra^{critical}$ increases as the dip decreases; the effect also depends on the aspect ratio, $HR = H_3/H_1$.

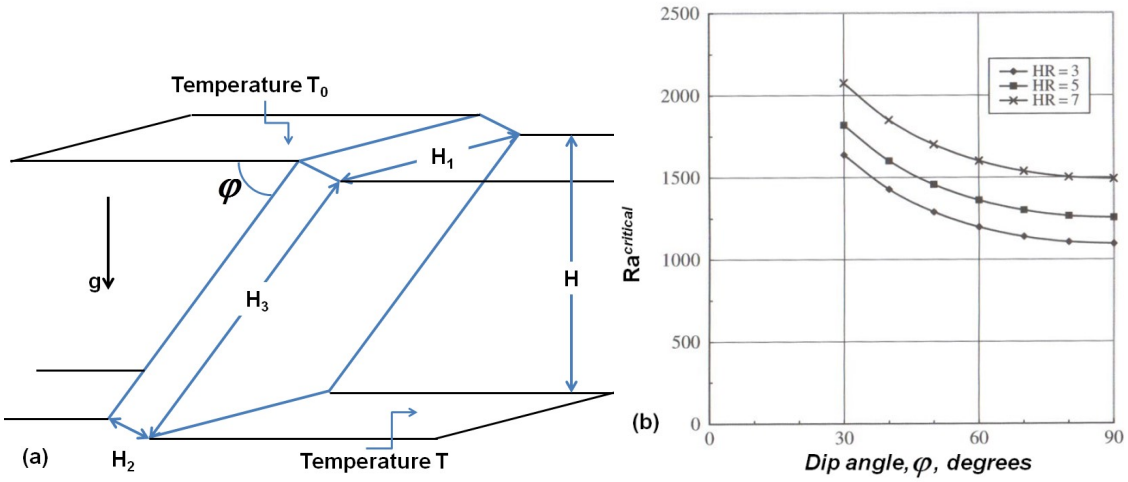

Figure 3.23. Thermal convection in an inclined fault. (a) Geometry of the problem. Dip angle is φ, temperature is fixed at top and bottom of a system of height, H, dimensions of the fault as shown. (b) Critical Rayleigh number for various dip angles drawn for the case of $H_2/H_3 = 0.1$. HR is the ratio H_3/H_1. For details of results for other geometries see Zhao et al. (2008).

3.5.3. Convective flow in over-pressured and flow-through systems.

In this section we outline the conditions for a flow system, in which the vertical fluid pressure gradient is super-hydrostatic, to become unstable and for fluid convection to initiate. Convection in systems with upward flowthrough driven by a fluid pressure gradient greater than hydrostatic is considered by Zhao et al. (2008). In contrast to the classical system where the temperatures and pressures are fixed at both the top and base where flow-through stabilises the flow (Jones and Persichetti, 1986), a system where the basal boundary conditions comprise fixed heat and mass fluxes (Figure 3.17 b) is destabilised by flow-through so that increases in $Pe^{thermal}$ increase the possibility of convection (Figure 3.24 (a) from Zhao et al. 2008). The Rayleigh number for such a system in which the temperature and fluid pressure is fixed at the top and a heat flux, q, and fluid flux are fixed at the base, is given by

$$Ra^{flux} = \frac{\left(\rho^{melt}\right)^2 c_P g \beta_T^{fluid} q K H^2}{\mu k_e^2} \qquad (3.48)$$

where β_T^{fluid} is the volumetric thermal expansion coefficient of the fluid.

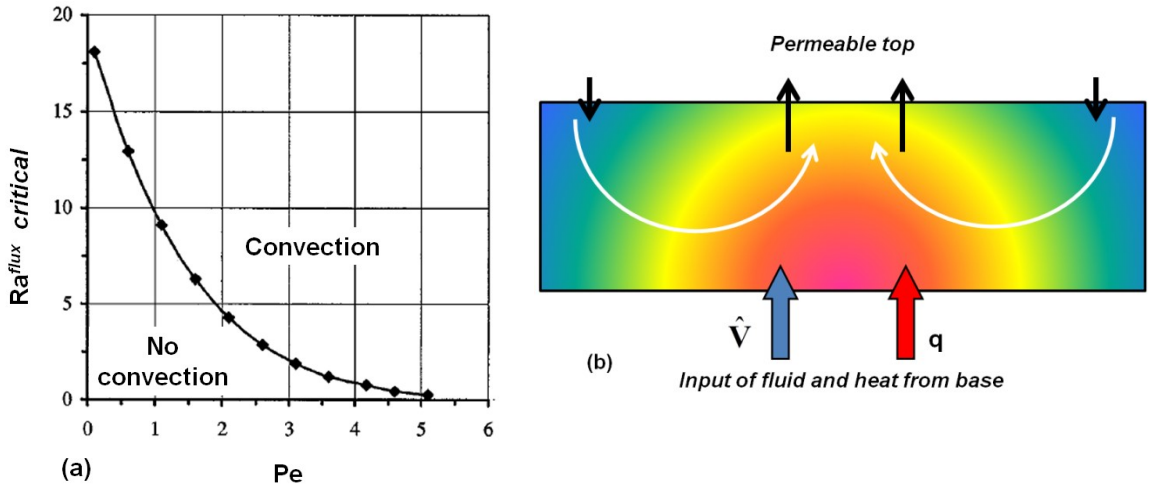

Figure 3.24. Convection in a system with flow-through. (a) Plot of $Ra^{flux}_{critical}$ against $Pe^{thermal}$ showing that increasing the upward flow-through in a system with open boundaries promotes instability. (b) Pattern of convection in a system with upward flow-through and input of heat at the base.

In §3.2.1 an example of a system is given where H = 10 km, q = 60 mW m^{-2}, the fluid pressure gradient is lithostatic and K = 10^{-18} m^2. This gives $Pe^{thermal}$ = 2.3 and Ra^{flux} = 5.3. Figure 3.24 (a) shows that these conditions are within the field where convection is possible for upward flow-through systems. Consider a situation where this 10 km thick compartment comprises the bottom part of a 40 km thick crust with a temperature gradient in the absence of fluid flow of 20 C^o km^{-1}.This means the temperature at the top of the compartment (at 30 km depth) is 600°C. At the base of the crust in the absence of thermal advection the temperature would be 800°C. Figure 3.10 and (3.24) show that for a Peclet number of 2.3, the temperature

at the base of the compartment is 3.9 times the conduction solution which means a temperature at the base of the compartment of 3120°C which is clearly unacceptable. Thus although convection is theoretically possible in this system the resulting temperature distribution that would arise is geologically unacceptable.

Convective flow in upward flow-through systems is slightly different to that developed in systems at an ambient hydrostatic pore pressure gradient in that the convective flow tends to reinforce or compete against the upward flow generated by the non-hydrostatic pressure gradient as shown in Figure 3.24 (b). Full convective rolls tend to develop in upward flow-through systems (Figure 3.25 c) for fluid pressure gradients close to hydrostatic as discussed by Zhao et al. (2008). This results in localised high velocity flow-through regions separated by lower velocity flow-through regions with elevated isotherms in the higher velocity regions. At least for systems close to the critical conditions for convective instability, the pattern is periodic in space with a horizontal wave number, k, given by (Zhao et al. 2008):

$$k = \frac{2\pi}{\lambda} = 1.74\left(1 - 0.18Pe\right)^{\frac{1}{4}} / \mathrm{H} \qquad (3.49)$$

where λ is the horizontal wavelength for the upwelling regions. For Pe = 1.0 and H = 10 km the resulting wavelength for the upwelling regions is 37.9 km. Examples of flow and temperature distributions in convective systems with flow-through for different values of Ra^{flux} and Pe are given in Zhao et al. (1999a, b, c). For the conditions represented in Figure 3.25 convection rolls form in the high permeability compartments (where the fluid pressure gradient is close to hydrostatic) with fluid drawn down to produce colder regions and upwards to produce hotter regions. In the low permeability compartments the flow is fairly uniform and upwards.

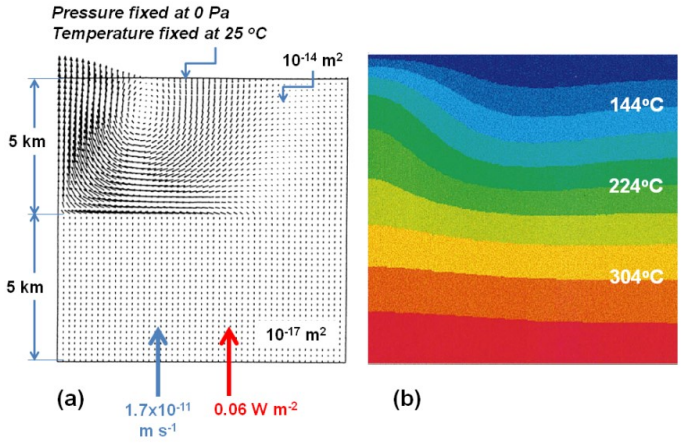

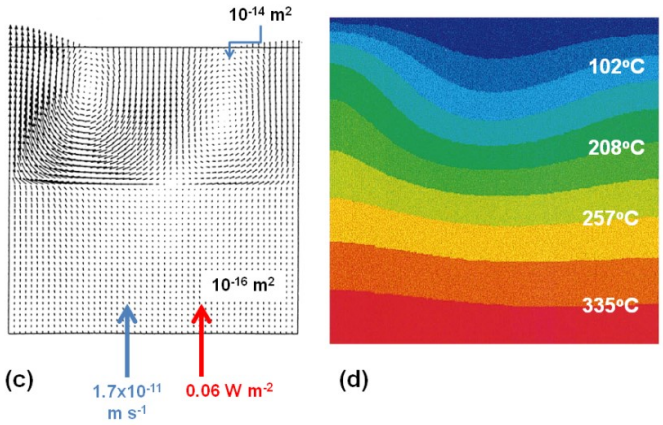

Figure 3.25. Two layer flow-through systems with convection. (a) Two compartments, lower one with K $=10^{-17}$ m^2 and upper, 10^{-14} m^2. Fluid pressure gradient in lower one lithostatic. Flow pattern is indicated in both compartments. (b) Temperature distribution corresponding to (a). (c) Two compartments, lower one with K $=10^{-16}$ m^2 and upper, 10^{-14} m^2. Fluid pressure gradient in lower one is below lithostatic. Flow pattern is indicated in both compartments. (d) Temperature distribution corresponding to (c). From Zhao et al. (2000).

Another statement of a principle that is proposed to govern the evolution of flow systems is given by Bejan (see Bejan and Lorente, 2011, Nield and Bejan, 2013 and references therein) and is commonly expressed as: *For a finite sized flow system to persist in time it must evolve in such a way that it provides easier and easier access to the currents that flow through it.* This is called the *Constructal Law* by Bejan who proposes it is as a universal law; there is continuing debate concerning the status of Bejan's proposal. This proposition is presumably related to entropy production extrema principles in some manner because it implies that the system will optimise its permeability structure to accommodate an imposed flow rate or maximise its flow rate for an imposed permeability structure.

One of the most instructive applications of extrema principles to flow controlled systems is that of Niven (2010) for flow in single and two (parallel) pipe systems. He shows that for a single pipe the Zeigler Maximum Entropy Production principle can be used as a selection criterion for the transition between laminar and turbulent flow. For a constant flow, two pipe system, a minimum entropy production principle can be used to define a stationary state for a given imposed flow and the Zeigler maximum entropy production principle still defines the transition from laminar to turbulent flow. In contrast, for a two pipe system with constant hydraulic head as the driving force the selection of flow regimes is based on a minimum entropy production criterion whereas the definition of stationary states is based on a maximum entropy production principle. These results offer the potential that similar selection rules could be developed for hydrothermal systems whereby a maximum entropy production principle may select between different modes of operation of the system (for instance fluidised versus non-fluidised flow) whereas a minimum entropy production principle may select different stationary states within each mode of operation.

3.6 Discrete fluid flow systems and percolation theory.

Fluid flow in hydrothermal systems occurs mainly by flow in fractures which have a multifractal geometry characterised by long range correlations (see Chapter 5). Continuum approaches, although capable of dealing with heterogeneous distributions of permeability, do not deal with long range correlations and are not concerned with the geometry of the

plumbing system associated with flow; by *geometry* is meant the details of the interconnections between fluid pathways and the shape and size distributions of these pathways. In order to deal with such detailed aspects of the plumbing system it is convenient to adopt an approach based on percolation theory which is a branch of statistical physics devoted to the study of phase transitions in heterogeneous materials (see Chapter 5) and associated aspects of fractal geometry, scaling and spatial correlations (Sahimi, 2011; Hunt et al., 2005). We present below one of the simplest applications of percolation theory to illustrate some aspects of criticality associated with a phase transition. The example involves percolation on a square lattice where the system undergoes a phase transition at a value of a probability parameter, p, equal to 0.59. We follow this model in Chapters 5 and 8 to illustrate other aspects of critical percolation theory. The model is particularly important in illustrating the principles behind ore body distribution at the regional scale.

In a percolation approach using a square lattice (Figures 3.26, 3.27, 3.28) the permeability at a particular point in the lattice is changed according to a probability, p, where $0<p<1$. In Figure 3.26 for instance p takes on values of 0.2 and 0.6 and at each point the permeability is changed from 10^{-18} m^2 to 10^{-15} m^2. Other values of p are shown in Figure 3.28. The theoretical value of p at which an infinite connected cluster arises in a square lattice is known as the critical probability, p_c, and for the two dimensional square lattice $p_c = 0.59$ (Hunt et al., 2005).

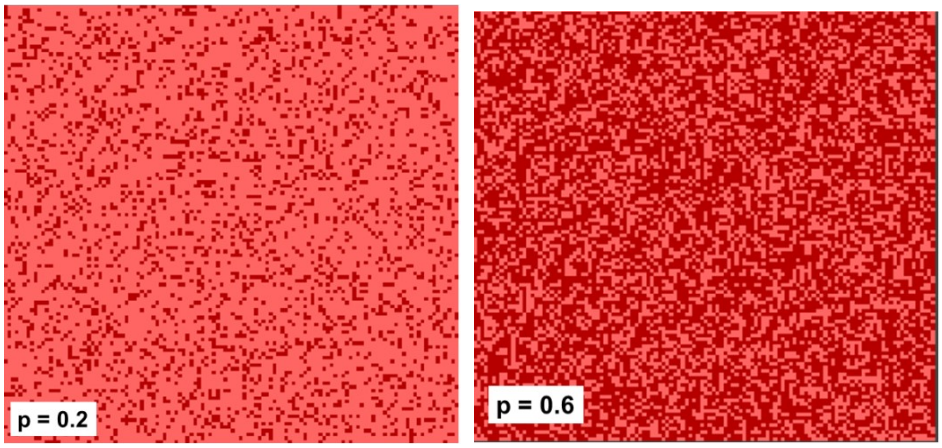

Figure 3.26 . A 120 x 120 square lattice with an initial homogeneous permeability of $10^{-18}m^2$ (pink) has the permeability changed at random to $10^{-15}m^2$ (red) according to a probability, p. Here we show results for p = 0.2 and p = 0.6 .

One important feature of The pattern of permeability at the critical value, p_c, is that the pattern is scale invariant at criticality. This means it is fractal. An important concept in the theory of critical systems is that of *renormalisation*. Renormalisation group theory is a form of *coarse graining* which involves spatial averaging so that small scale structure is removed whilst preserving the larger length scale structure. The process is particularly important is systems where many length scales are present. In Figure 3.27 the renormalisation concept is illustrated. Figure 3.27 (a) shows a 9 x 9 square latice with some squares marked blue and some white. If we subdivide this iamage into 3 x 3 blocks and recolour the new squares according to the majority colour in each 3 x 3 block we obtain Figure 3.27 (b). If we shrink this image to obtain Figure 3.27 (c) then we see that Figure 3.27 (c) is statistically

similar to a 3 x 3 block in Figure 3.27 (a). In other words the pattern in Figure 3.27 (a) is scale invariant.

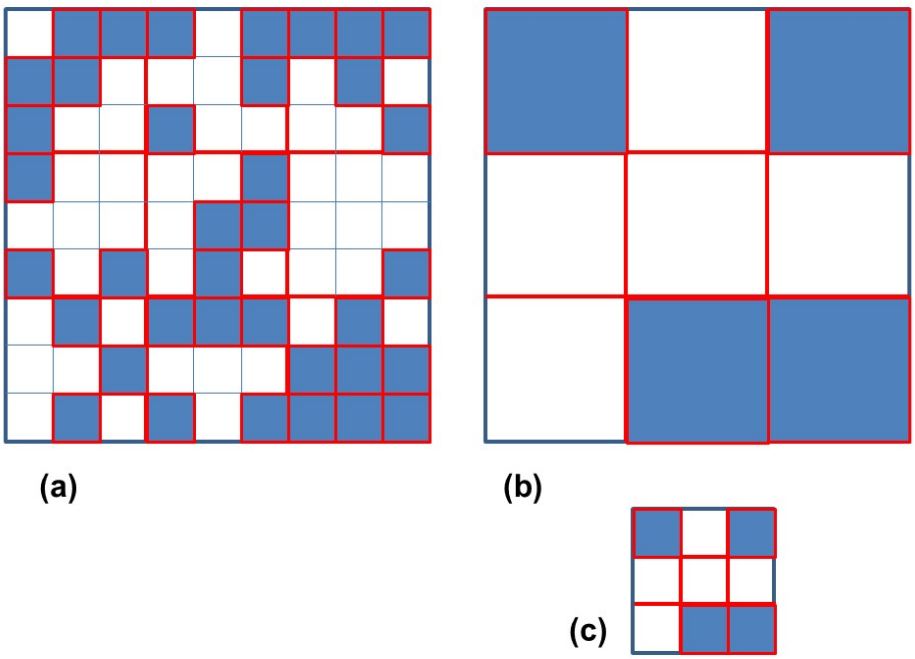

Figure 3.27. An illustartion of group renormalisation theory. The 9 x 9 image in (a) is transformed to the image in (b) by taking each 3 x 3 block in (a) and replacing it by the majority colour in that block. The resulting image in (b) shrinks to the 3 x 3 image in (c) which is statistically similar to some 3 x 3 blocks in (a).

In Figure 3.28 we apply this same renormalisation transformation to our permeability images for p = 0.8, p = 0.6, and p = 0.3 with the initial image being 81 x 81 in size. We see that as the transformation continues to smaller and smaller scales the pattern for p = 0.8 flows to a uniform permeability value of 10^{-15} m^2 whereas the image for p = 0.3 flows to a uniform permeability value of 10^{-18} m^2. The image close to criticality flows to images that are statistically similar to the original distribution. Thus the pattern at criticality (p ~ 0.6) is fractal and scale invariant. We examine critical systems in greater detail in Chapter 5.

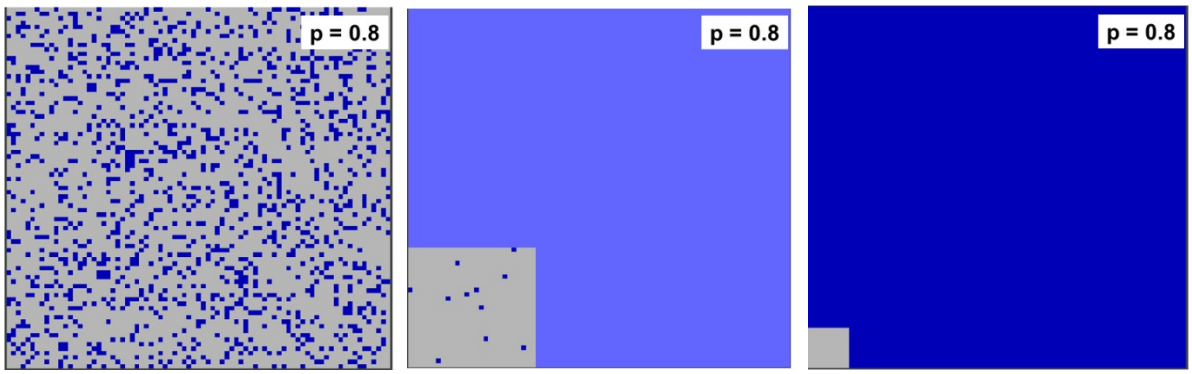

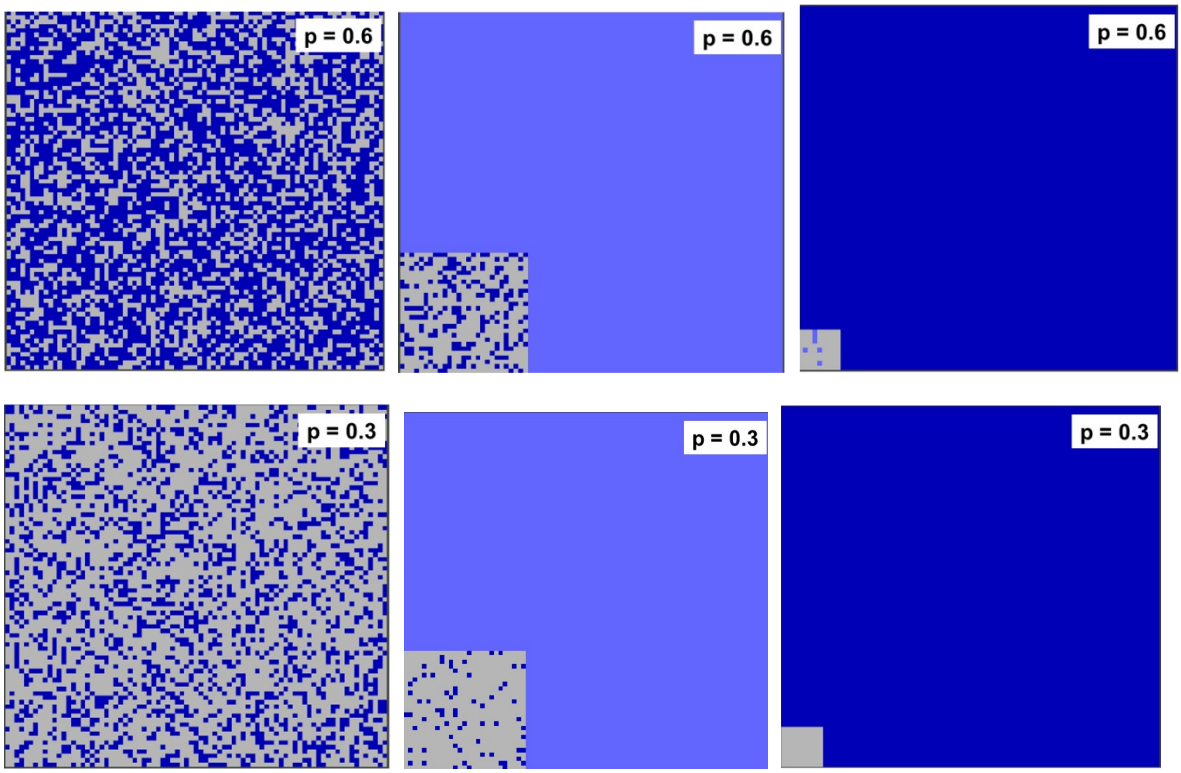

Figure 3.28. Group renormalisation applied to permeability distributions for different values of the probability, p. For $p = 0.8 > p_c$ the renormalisation procedure flows to a uniform distribution. This is also true for $p = 0.3 < p_c$. For $p = 0.6 \cong p_c$ the pattern flows to self-similar versions of the original. Thus at criticality the pattern of permeability is fractal.

For an array of connected fractures the network is characterised by a probability distribution of fractures apertures and for a given network one can identify the smallest aperture (or throat) in the array. The volumetric flow through the network is limited by the size of that throat and is proportional to the cube of the aperture size. The main result of discrete theory applied to arrays of fractures is that once the percolation threshold is reached the flow through the system is controlled by that connected fracture pathway that has the largest small throat.

The application of the principles of discrete flow systems is particularly relevant to systems that range in size from microns to perhaps 10's of meters. Here individual fractures can be mapped and models of the fracture networks generated. At larger length scales this becomes impractical and one approach is to delineate regions with different degrees of fracturing (and hence permeability) and treat these as though the flow is averaged and hence described by Darcys law. It is then possible to apply percolation theory at the regional scale.

As an example of percolation theory applied to flow systems we present in Figures 3.29 and 3. 40 some examples of spatial permeability distributions and resulting flow patterns developed at a regional scale in two dimensions. The example is meant to represent a vertical fault plane 30 km long and 30 km high divided into elements 200 m on edge. The initial permeability is set at 10^{-18} m^2 so that with a lithostatic fluid pressure gradient, the vertical Darcy flow is negligible at 1.7×10^{-12} m s^{-1}. We imagine that fracture systems develop within the fault and these fractures induce a local permeability of 10^{-15} m^2 at random within elements with a probability of formation equal to p. We develop a permeability network by assigning

this new permeability at random for each element in the system. The patterns of permeability networks developed for p = 0.2, 0.3, 0.6, 0.8 are shown in Figures 3.26 and 3.28.

There are a number of important characteristics of these networks. We consider some of these below but revisit the example again in Chapter 5; the example illustrates many important features of critical systems.

(i) The spatial distribution of sites with high permeability is multifractal; we present analyses of these figures in Chapters 5.

(ii) For probabilities below and equal to 0.6 there is no continuous low permeability network across the system so that the system remains with low permeability.

(iii) By p = 0.8 continuous permeability networks have formed across the system. The theoretical value of p for the percolation threshold, p_c, for this array is 0.59 (Sahimi, 2011).

(iv) In Figure 3.29 we impose a fluid flux of 2.65 x 10^{-11} ms^{-1}. For an initial permeability of 10^{-18} m^2 this flux corresponds to a lithostatic fluid pressure gradient throughout the system with the base of the system at 30 km. The patterns of fluid flow are shown as streamlines. The streamlines begin at p = 0.1 as close to uniformly distributed with only local departures from uniform arising from focussing in high permeability regions. This inhomogeneity grows as p increases until by p = 0.4 and p = 0.6 the flow is focussed into well-defined zones. After p = 0.6 this trend reverses and by p = 0.9 the flow approaches uniformity again. In Chapter 8 we couple these fluid flow systems with chemical reactions.

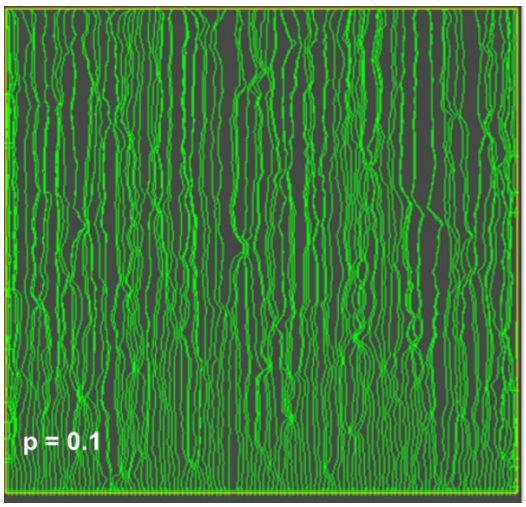

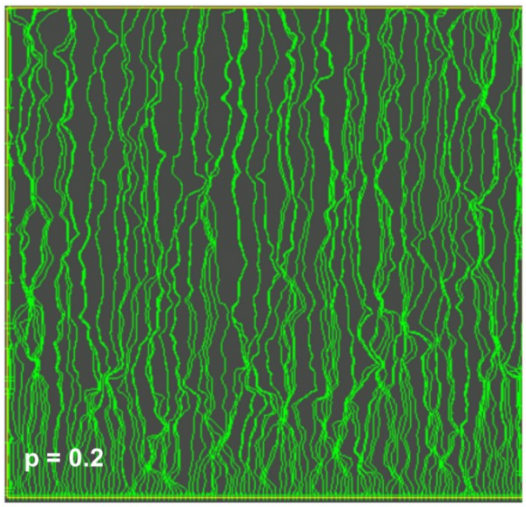

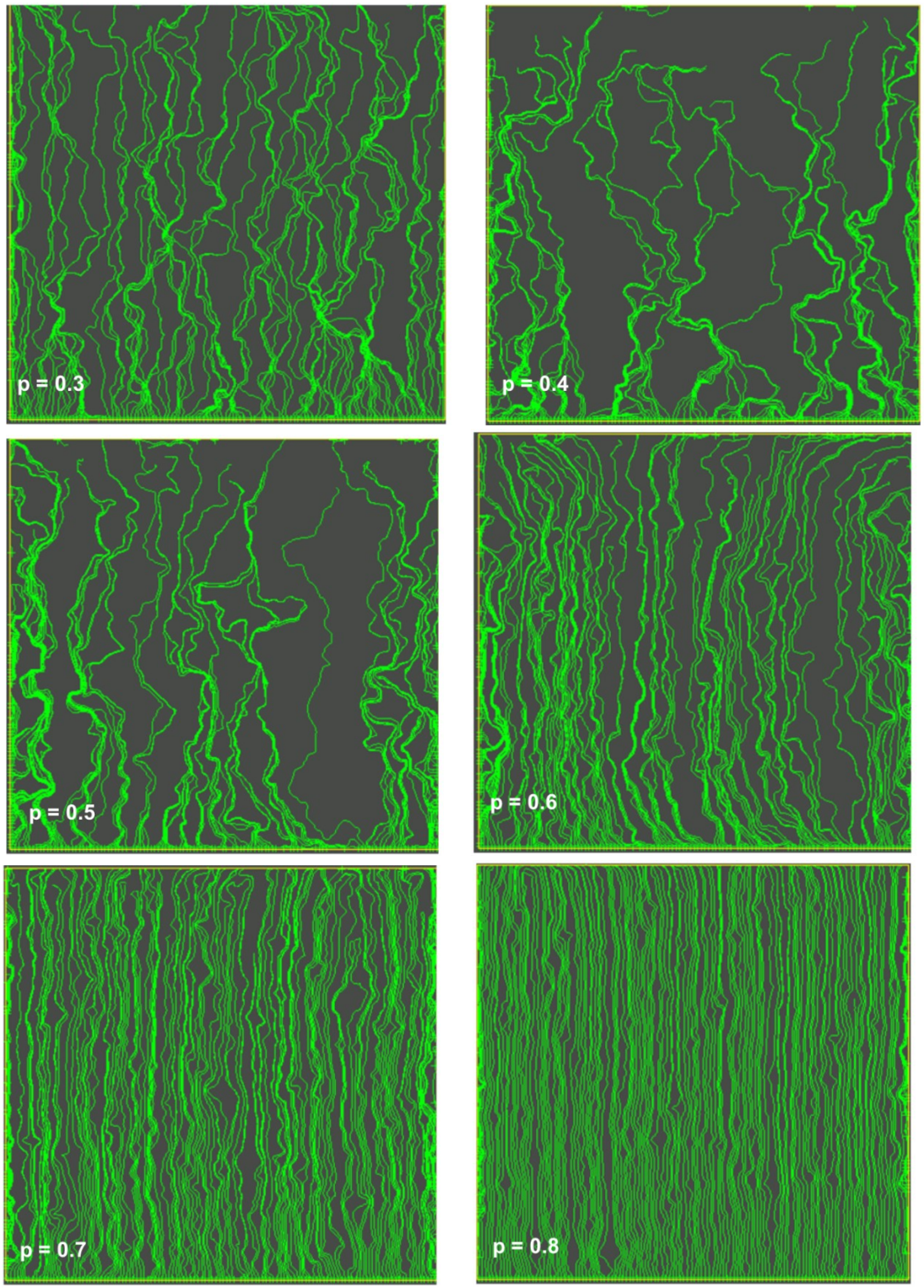
p = 0.3
p = 0.4
p = 0.5
p = 0.6
p = 0.7
p = 0.8

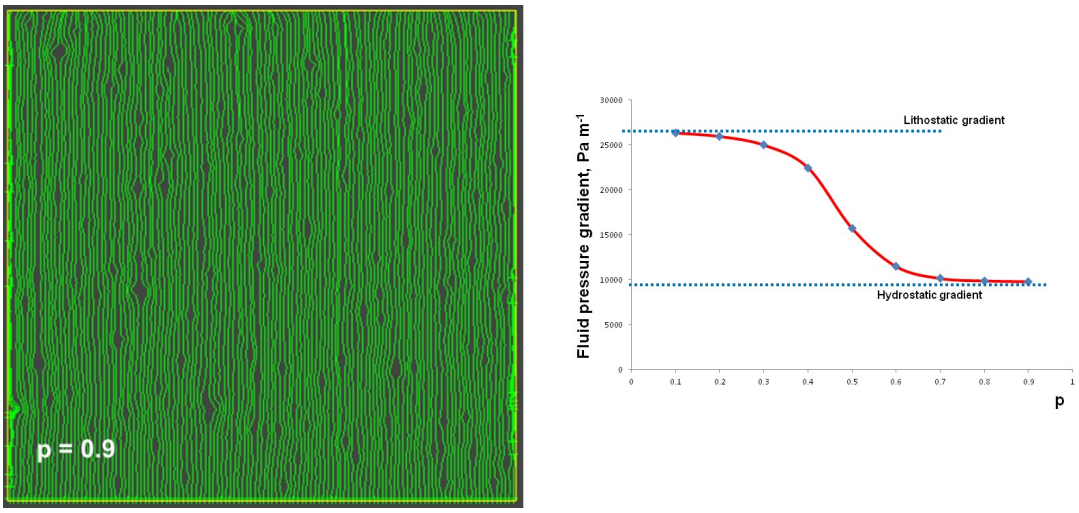

Figure 3.29. Streamline distributions for various values of the probability, p. In the lower right diagram the variation of the fluid pressure gradient with p is plotted. At low values of p the fluid pressure gradient is close to lithostatic. As p increases the fluid pressure gradient decreases and finally collapses toward a hydrostatic gradient as more and more of the imposed fluid flow is taken up by high permeability regions. This pattern of behaviour is mirrored in the streamline patterns.

(v) At low values of p the fluid pressure gradient is close to lithostatic. As p increases the fluid pressure gradient decreases and finally collapses toward a hydrostatic gradient at $p = p_c$ as more and more of the imposed fluid flow is taken up by high permeability regions. This pattern of behaviour is mirrored in the streamline patterns.

(vi) If one plots the magnitudes of the Darcy velocity for this same sequence (Figure 3.40) the same trend is indicated with the maximum Darcy velocity reaching a maximum just before $p = p_c$ for large systems.

We emphasise that the reuslts presented here for critical permeability networks contrast with those where the boundary conditions consist of imposed fluid pressures at the top and bottom of the ystem. If the fluid pressure gradient is fixed,a system we consider to require the intervention of a Mazwell Demon and is therefore thermodyanmically inadmissable in the Earth, then maximum fluid flow occcurs *at and after criticality* as the density of intercnnected fluid pathways increases. As we have indicated, for fixed fluid flux at the base of the system, the maximum Darcy velocity increases and reaches a maximim *before criticality* and decreases as the density of interconnected fluid pathways increses after criticality.

For fixed fluid flux boundary conditions, the system cannot support the low fluid pressure columns in a system 35 km high with gravity and so, after criticality, must collapse back to an array of compartments with critical heights given by (3.3). The system then has a subcritical permeability distribution and can support a lithospheric pressure gradient but then evolves again towards ctriticallity. Thus the flow system oscillates with time as the system continuously evolves through ctriticallity. We explore this system further in Chapter 5.

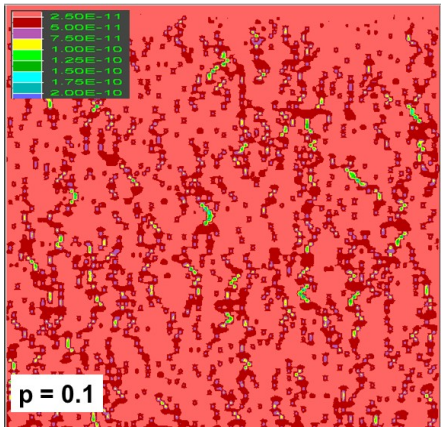
2.50E-11
5.00E-11
7.50E-11
1.00E-10
1.25E-10
1.50E-10
1.75E-10
2.00E-10
p = 0.1

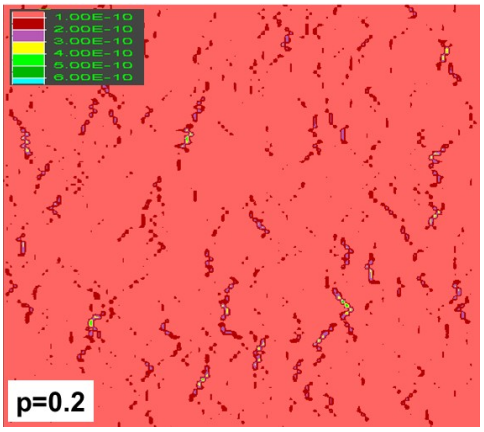
1.00E-10
2.00E-10
3.00E-10
4.00E-10
5.00E-10
6.00E-10
p=0.2

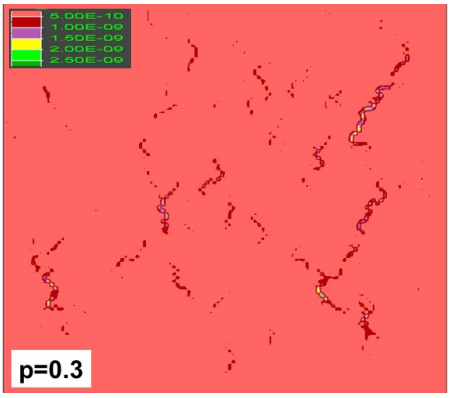
5.00E-10
1.00E-09
1.50E-09
2.00E-09
2.50E-09
p=0.3

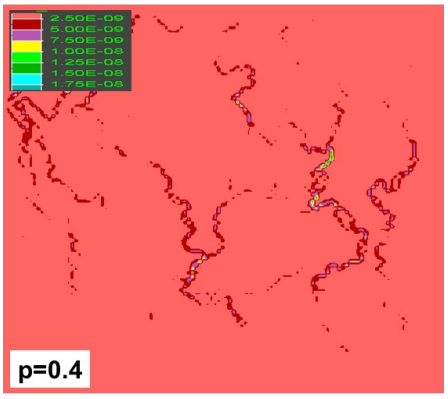
2.50E-09
5.00E-09
7.50E-09
1.00E-08
1.25E-08
1.50E-08
1.75E-08
p=0.4

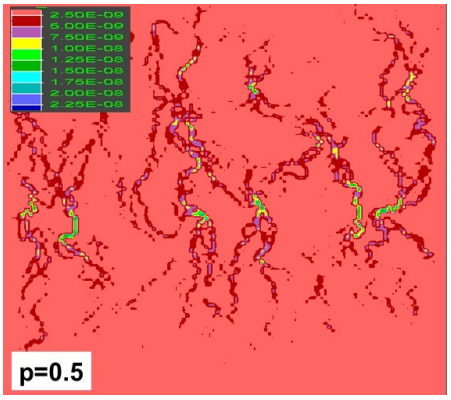
2.50E-09
5.00E-09
7.50E-09
1.00E-08
1.25E-08
1.50E-08
1.75E-08
2.00E-08
2.25E-08
p=0.5

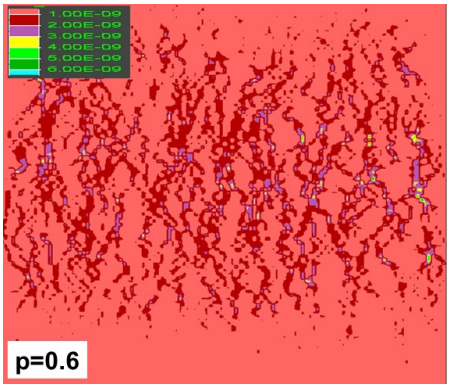
1.00E-09
2.00E-09
3.00E-09
4.00E-09
5.00E-09
6.00E-09
p=0.6

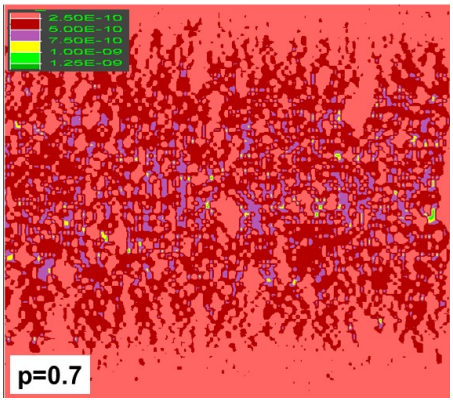
2.50E-10
5.00E-10
7.50E-10
1.00E-09
1.25E-09
p=0.7

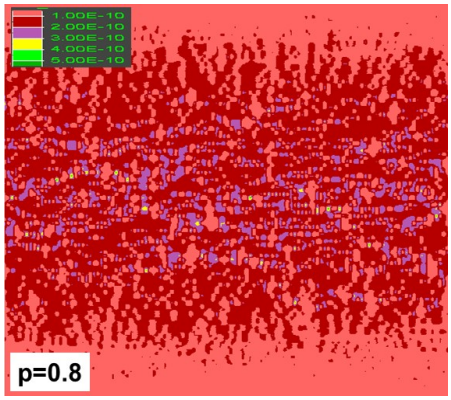
1.00E-10
2.00E-10
3.00E-10
4.00E-10
5.00E-10
p=0.8

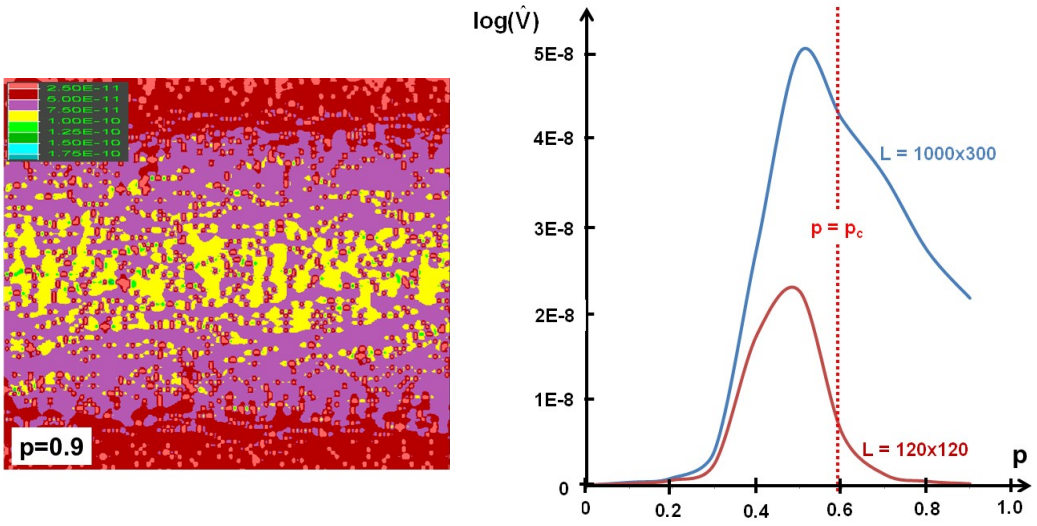

Figure 3.30. Patterns of Darcy velocity magnitudes, $\hat{V}$ (in units: m s^{-1}), for various values of the probability, p. The legend for velocity is shown in each image. In the lower right diagram the logarithm of the maximum value of these velocities is plotted as a function of p. The maximum velocity reaches a maximum (more than two orders of magnitude above that at p = 0.1) at p = 0.5 just as the pore pressure gradient is collapsing as shown in Figure 3.29. Thus maximum flow velocities are reached before criticality. The diagram illustrates finite size effects.

3.7. Overview of hydrothermal plumbing systems.

Partly as a summary of this chapter we develop a model for crustal plumbing systems based on the principles developed here. Similar arguments to those presented above have been developed for silicate melt systems by Hobbs and Ord (2010). The basic principles that govern the patterns of fluid flow and the thermal structure of the crust are:

(i) The continuity equation (3.16) must be honoured throughout a metasomatic system. This means that for systems in which there is no internal source or sink for fluids and if the horizontal Darcy flux component, $\hat{V}_x$ is zero then if the upward flux, $\hat{V}_y$, is zero at any point in such a system then $\hat{V}_y = 0$ everywhere. Hence a hydrostatic fluid pressure gradient at any point in the system demands a hydrostatic fluid pressure gradient throughout the system. Conversely a non-zero upward Darcy flux at one point in the system demands a non-zero flux everywhere.

(ii) For a layered crust the lowest permeability layer acts as a fluid pressure control valve for the flux of fluid through the rest of the crust. If the fluid pressure gradient is lithostatic in this layer, continuity of flux (see (3.16)) demands that the fluid pressure gradient be less than lithostatic in higher permeability layers, shear zones or lenses. A factor of 10 increase in permeability contrast is enough to reduce the fluid pressure gradient in the higher permeability layer to within 20% of hydrostatic. This fluid pressure gradient distribution is solely a result of changes in permeability and is independent of any need for low permeability "seals" or "caps". Continuity of fluid flux defines the permissible distributions of fluid pressure gradients in a layered crust as shown in Figure 3.12.

(iii) The same principles as in (ii) apply to dipping fault or shear zones so that if the permeability is high within the fault zone the fluid pressure gradient will be close to hydrostatic even though the fluid pressure gradient in the surrounding rocks is lithostatic.

(iv) Fluid is focussed into high permeability layers or lenses. The focussing factor can be greater than an order of magnitude for a permeability contrast of 10 (Figure 3.20). This means that for many systems most of the fluid is diverted from low permeability regions and focussed into high permeability faults, shear zones or fracture networks.

(v) A crustal compartment where the fluid pressure gradient is close to hydrostatic is restricted in height because of the stresses produced at the base and top of the compartment. This places restrictions on the height of compartments and of high permeability faults and shear zones as defined by (3.3).

(vi) The patterns of convection that develop in crustal compartments with fluid flow-through depend on the boundary conditions for thermal and fluid fluxes. For such systems with impermeable upper and lower boundaries, thermal convection cannot occur. If the upper and lower boundaries allow fluid fluxes, and the base is a heat flux boundary, fluid convection is possible, in principle, even for a lithostatic fluid pressure gradient but only if the Peclet number is less than about 5. We will see below that for a lithostatic pressure gradient the value of the Peclet number places severe restrictions on the possibility of thermal convection in natural geological settings.

(vii) The patterns of convection that develop in high permeability faults and shear zones is invariably three dimensional in that both upward and downward flow regions develop forming a finger-like pattern (figure 3.26). This means that two dimensional sections through such systems are inadequate to show the true patterns of fluid circulation and temperature distribution.

(viii) Topographic gradients are important in driving substantial horizontal components of fluid flow (including surface derived fluids, over-pressured fluids and melts) especially if the relief is large. Such processes are also capable of driving surface derived fluids to at least mid-crustal levels.

(ix) Fluid flow is always driven by gradients in pore fluid pressure. This statement needs to be modified if a gravity field is important so that the driving force becomes a gradient id hydraulic head. The mean stress is proportional to the fluid pressure only in elastic materials or in elastic-viscous-plastic materials where there is no viscous-plastic volume changes. In most materials of interest in hydrothermal systems fluid flow is driven by gradients in viscous-plastic volume changes; these gradients by far outweigh any gradients in mean stress.

(x) It is important to understand the different behaviours of systems that have fluid pressures as boundary conditions as opposed to systems that have fluid fluxes as boundary conditions. Different convective patterns and fluid flow distributions result from the different boundary conditions. For most systems fluid pressure boundary conditions are thermodynamically inadmissible for the Earth since they require work to be done by some convenient entity (a Maxwell Demon) in order to maintain the imposed fluid pressures. In particular, an evolving permeability distribution reaches maximum fluid velocities before criticality for flux boundary conditions and after criticality for fluid pressure boundary conditions. Large systems with flux boundary conditions must

oscillate through criticality as the system evolves and the pore fluid pressure gradient oscillates between lithostatic and close to hydrostatic at criticality.

There are three end-member models of the fluid flow-thermal structure of metasomatic systems. One is typified by the model presented by Etheridge et al. (1983) where convection dominates in the lower half of the crust and the permeability of the crust is relatively high (say > 10^{-16} m^2) controlled by fracture permeability. Another is typified by the models of Lyubetshaya and Ague (2009) where no convection occurs, the flow is essentially upwards, although influenced by topography, and the permeability of the lower crust is low (≈ 10^{-19} m^2); localised fluid flow occurs in shear zones or narrow zones of lower permeability. The third type of model, typified by Oliver (1996) and summarised in Figure 3.1, is similar to that of Lyubetshaya and Ague (2009) but the role of localised flow is emphasised; this third model is presumably the one applicable to orogenic gold deposits.

With the ten basic principles outlined above in mind, the question is: *Which of these models is more likely in metasomatic systems*? A related issue concerns the fault valve and seismic pumping models of Sibson (1994) and Cox (1995, 1999). In view of the flux continuity constraints imposed by (3.16) *what are the conditions under which the fault valve mechanism can operate?*

Each of the models has its own implications for the thermal structure of the crust. We take as a first order observation that there are no major discontinuities in the crust where the temperature gradient suddenly increases dramatically. The temperature within metasomatic systems is clearly elevated with respect to adjacent regions in the crust but overall the temperature structure is what one would expect from elevated heat flow from the mantle or from changes in the thickness of the crust (Chapter 2). Overall the temperature distribution is similar to what one would expect from a model that involves simple conduction of heat. Above all, the temperature at the Moho is limited to perhaps 1000°C to 1200°C as a maximum at about 40 km depth (corresponding to a mean temperature gradient of 25 C^o km^{-1} to 30 C^o km^{-1}). If one is prepared to accept these first order approximations to the thermal structure of metasomatic systems then major constraints are placed on the advection of heat vertically carried by moving fluids.

In a system where the fluid pressure gradient is lithostatic, fluids flow upwards unless influenced by a topographic gradient. Figure 3.13 shows that for such a fluid pressure gradient, high values of the Peclet number (say 5) result in large temperature gradients at the top of the system and grossly elevated temperatures (≈ 30 times the conduction solution) at the base of the system. The observations point to a maximum Peclet number closer to one, that is, close to the conduction solution that one would expect from elevated heat flow of thickened crust. In fact Pe = 1 is an upper limit for the physically possible Peclet number since it gives a temperature at the base of the system of 1.7 times the conduction solution. For hot crustal conditions Pe < 1 is more compatible with observations.

If we assume Pe = 1 and use the values for water from Table 3.1 for a compartment with a lithostatic fluid pressure gradient then

$$\mathrm{Pe} = 1 = \frac{\mathrm{H}\rho_0^{fluid}\mathrm{c_P}}{k_e}\hat{\mathrm{V}} = \frac{10^4 \mathrm{x} 10^3 \mathrm{x} 4185}{3.08}\hat{\mathrm{V}}$$

which gives $\hat{V} = 7.36x10^{-11}$ m s^{-1}. Again this is an upper limit for the Darcy flux. Connolly (2010) using a different argument arrives at a value for the Darcy flux in metamorphic systems of $\approx 10^{-12}$ m s^{-1}. Accepting the above value of $\hat{V}$ and using Darcy's law we obtain

$$K = \mu^{fluid}\hat{V}\left(\nabla\mathcal{H}\right)^{-1} = \frac{10^{-4}x7.36x10^{-11}}{1.7x10^{4}} = 4.33x10^{-19}\,m^2$$

This value of the permeability agrees well with the value 10^{-19} m^2 assumed by Lyubetshaya and Ague (2009); Connolly (2010) arrives at a permeability value of 10^{-20} m^2. We now ask: *What value of thermal flux is necessary to initiate convection in this system*? For Pe = 1, Figure 3.28 (a) says we need a Rayleigh number greater than 10 to initiate convection. Hence we write

$$q = \frac{Ra\mu^{fluid}k_e^2}{\left(\rho_0^{fluid}\right)^2 H^2 c_P g\beta_T^{fluid} K} = \frac{10x10^{-4}x(3.08)^2}{10^6 x10^8 x4185x9.8x2.01x10^{-4}x4.33x10^{-19}}$$

from which we obtain q = 26.6 W m^{-2}. This is about four orders of magnitude larger than the average crustal heat flow of 60 mW m^{-2}. Reducing Pe to 0.1 increases q to 266 W m^{-2} and increasing Pe to 2 gives q = 13.3 W m^{-2}. Hence we reach the conclusion that for realistic heat flows and a thermal structure that is near the conduction solution, thermal convection is not possible in a system with a lithostatic fluid pressure gradient. Although others have reached the same conclusion (Wood and Walther, 1986; Oliver, 1996) this argument is based on strict thermal-hydrological arguments for systems with upward fluid flow-through.

If however a more permeable compartment develops in the crust then even though the surrounding rocks maintain a lithostatic fluid pressure gradient, the fluid pressure gradient (from (3.20)) must be less than lithostatic in order to maintain continuity of fluid flux. As we have seen even a 10-fold increase in permeability is sufficient to decrease the fluid pressure gradient in the high permeability compartment to within 20% of hydrostatic. If indeed the fluid flow regime in metasomatic systems is characterised by Peclet numbers close to one then the permeability in such systems is close to 10^{-19} m^2 which is close to the percolation thresh-hold (Meredith et al., 2012). As such even a small change in porosity (from 0.01 to 0.05) resulting from deformation or chemical reactions can induce a permeability increase of several orders of magnitude.

The limitation on the height of such high permeability compartments is that it must be less than the critical height defined by (3.3). This means that high permeability shear zones can form and persist with a near hydrostatic fluid pressure gradient as long as the thickness of the shear zone measured vertically is less than the critical height. For instance, a shear zone with $\overline{\sigma}^{tensile}$ = 10 MPa and $\overline{\sigma}^{compressive}$ = 30 MPa has a critical height of 1.77 km. If the dip of the shear zone is 30^o the true thickness of a zone that persists with a hydrostatic fluid pressure gradient is 1.5 km. The geometry is shown in Figure 3.31. Figure 3.23 (b) shows that the critical Rayleigh number for a zone with 30^o dip and an aspect ratio of 3 is about 1650.

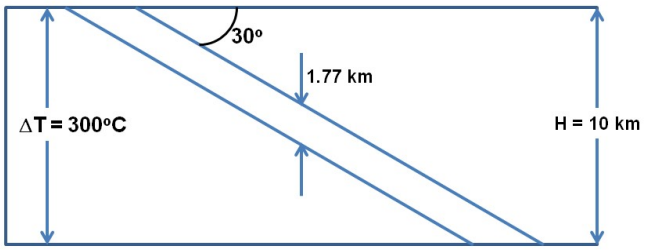

Figure 3.31. Model of shear zone dipping at 30° in a 10km thick compartment.

If we calculate the Rayleigh number for this fault from (Zhao et al., 2008, p 178):

$$\mathrm{Ra} = 1650 = \frac{\left(\rho_0^{fluid}\right)^2 c_P g \beta_T^{fluid} \Delta T K H}{\mu^{fluid} k_e} = \frac{10^6 \mathrm{x} 4185 \mathrm{x} 9.8 \mathrm{x} 2.1 \mathrm{x} 10^{-4} \mathrm{x} 300 \mathrm{x} 10^4}{10^{-4} \mathrm{x} 3.08} K$$

Or, $K = 1.97 \times 10^{-14}\ m^2$

Thus we reach the conclusion that unless the permeability is increased in shear zones (dipping at 30°) to above 10^{-14} m^2 then convection is not possible even in such zones. If we maintain the aspect ratio and increase the dip to 60°, the true thickness for a shear zone that can maintain a hydrostatic fluid pressure becomes 0.89 km and the permeability required to initiate convection is 1.43×10^{-14} m^2.

The overall conclusion is that fluid convection systems are not possible in compartments with lithostatic fluid pressure gradients under geological conditions. If the permeability in a compartment overlying the compartment with a lithostatic gradient is about 10^{-14} m^2 or greater then convection is possible in that compartment depending on its height which must be less than or equal to the critical height. Such high permeabilities in metasomatic systems at high crustal levels are reasonable.

Recommended reading.

Coussy, O., 1995. *Mechanics of Porous Continua*. Wiley, Chichester, UK.

Coussy, O., 2004. *Poromechanics*. Wiley, Chichester, UK.

These are the definitive books on the thermodynamics of porous media. Both of these books treat the flow of fluids through deforming porous media. The 1995 version is more complete and thorough and includes both Eulerian and Lagrangian treatments of the fluid flow; the 2004 version is easier to read. Deformation topics include poro-elasticity and plasticity. Coupling to chemical reactions and phase changes are included.

Coussy, O., 2010. *Mechanics and Physics of Porous Solids*. Wiley, Chichester, UK.

This book treats classical thermodynamics from the viewpoint of someone interested in flow through porous media. It provides an interesting different look at classical thermodynamics.

Hunt, A., Ewing, R., and Ghanbarian, B. 2014. *Percolation Theory for Flow in Porous Media*. Springer.

Nield, D. A., and Bejan, A. 2013. *Convection in Porous Media*. Springer-Verlag.

This is the definitive book on thermal and mixed convection in porous media.

Phillips, O.M., 1991. Flow and Reactions in Permeable Rocks. Cambridge University Press, Cambridge.

An important and easily readable book on fluid flow through porous media. It is written from a geologist's viewpoint and includes equilibrium treatments of chemical reactions coupled to advection.

Phillips, O.M., 2009. Geological Fluid Dynamics: Sub-surface Flow and Reactions. Cambridge University Press, Cambridge.

This is a second version of Phillips (1991) and is not as complete as the earlier version.

Sahimi, M. Flow and transport in Porous Media

Sahimi, M., Gavalas, G., and Tsotsis, T. T. 1990. Statistical and continuum models of fluid-solid reactions in porous media. Chem. Eng. Sci., 45, 1443- 1502.

A comprehensive review of fluid solid chemical reactions in porous media from both continuum and percolation viewpoints.

Zhao, C., Hobbs, B. E., and Ord, A. 2008. *Convective and Advective Heat Transfer in Geological Systems*. Springer.

This book presents a thorough treatment of the mathematical background to fluid flow in hydrothermal systems including fluid focussing, thermal convection in faults and thermal convection in systems with flow-through.